entropy

MDPI

Article

Auto- versus Cross-Correlation Noise in Periodically Driven Quantum Coherent Conductors

Michael Moskalets

Department of Metal and Semiconductor Physics, NTU "Kharkiv Polytechnic Institute", 61002 Kharkiv, Ukraine; michael.moskalets@gmail.com

Abstract: Expressing currents and their fluctuations at the terminals of a multi-probe conductor in terms of the wave functions of carriers injected into the Fermi sea provides new insight into the physics of electric currents. This approach helps us to identify two physically different contributions to shot noise. In the quantum coherent regime, when current is carried by non-overlapping wave packets, the product of current fluctuations in different leads, the cross-correlation noise, is determined solely by the duration of the wave packet. In contrast, the square of the current fluctuations in one lead, the autocorrelation noise, is additionally determined by the coherence of the wave packet, which is associated with the spread of the wave packet in energy. The two contributions can be addressed separately in the weak back-scattering regime, when the autocorrelation noise depends only on the coherence. Analysis of shot noise in terms of these contributions allows us, in particular, to predict that no individual traveling particles with a real wave function, such as Majorana fermions, can be created in the Fermi sea in a clean manner, that is, without accompanying electron–hole pairs.

Keywords: single-electron wave packet; shot noise; quantum transport

Citation: Moskalets, M. Auto- versus Cross-Correlation Noise in Periodically Driven Quantum Coherent Conductors. *Entropy* **2021**, *23*, 393. https://doi.org/10.3390/e23040393

Academic Editor: Dario Ferraro

Received: 26 February 2021
Accepted: 23 March 2021
Published: 25 March 2021

1. Introduction

Recently, the quantum tomography of a single-electron wave function was demonstrated experimentally [1,2]. In both experiments, a periodic stream of single-electron wave packets was mixed with a low-amplitude electrical probe signal at the electron wave splitter, a quantum point contact, and the resulting electrical noise averaged over long time was measured. However, if the fluctuations of an electrical current within one output lead were measured in one experiment, the correlations of currents flowing within both output leads were measured in another. In a sense, these works are the culmination of a number of recent works where the cross-correlation noise was measured to count electrons emitted per period [3,4] to demonstrate a tunable fermionic anti-bunching [4–7], and the auto-correlation noise at high [8,9] and low [10,11] frequencies was measured to identify a single-electron emission regime. These experimental advances motivate us to take a closer look at how exactly the quantum properties of wave packets manifest themselves in the measured electrical noise [12–14].

Note that tomography of the density profile of solitary electrons was successfully realized in [15] using the measurement of the electrical current rather than noise.

Here, in contrast to previous works [16–32]—for a review, see in [33]—I will focus on comparing auto- and cross-correlation noise. I will show that, in the case of a periodic train of non-overlapping single-electron wave packets scattered off the wave splitter with reflection probability R, there are two contributions to noise. These contributions can be addressed separately by measuring both auto- and cross-correlation noise in the weak back-scattering regime, $R \ll 1$. As I will show in the subsequent sections, for a single-electron wave packet $\Psi(t,x) = e^{-\frac{i}{\hbar}\mu t}\psi(t,x)$ injected during one period into a one-dimensional chiral Fermi sea and reflected into a detector at a wave splitter, see Figure 1, the auto-

correlation, $\mathcal{P}^{ex}_{auto}$, and cross-correlation, $\mathcal{P}_{cross}$, noise power, see Equation (10), at frequency ω and at zero temperature are calculated as follows:

$$\begin{aligned} \mathcal{P}^{ex}_{auto}(\omega) &= R\frac{e^2}{\mathcal{T}_0}\int\limits_{-\infty}^{\infty} d\tau e^{i\omega\tau}\frac{\mathrm{Im}\,\mathcal{C}(\tau)}{\pi\tau}, \\ \mathcal{P}_{cross}(\omega) &= -R\frac{e^2}{\mathcal{T}_0}|\mathcal{N}(\omega)|^2, \end{aligned} \tag{1}$$

where the superscript ex (unnecessary for cross-correlation noise) indicates the excess over the equilibrium value, e is an electron charge, $\mathcal{T}_0$ is a period, $\mathcal{C}(\tau)$ is the integrated over time coherence of the wave function envelope, [34,35]

$$\mathcal{C}(\tau) = \int\limits_{-\infty}^{\infty} dt\psi^*(t+\tau, x_D)\psi(t, x_D), \tag{2}$$

and $\mathcal{N}(\omega)$ is the Fourier transform of the wave packet density,

$$\mathcal{N}(\omega) = \int\limits_{-\infty}^{\infty} d\tau e^{i\omega\tau}|\psi(\tau, x_D)|^2. \tag{3}$$

In Equations (2) and (3), x_D is the coordinate of the detector used to measure the current. For simplicity, I assume that the coordinates of both detectors in the outgoing channels $\alpha = 3$ and $\alpha = 4$ are the same. Below, I discard x_D and use the following notation: $\Psi(t) \equiv \Psi(t, x_D)$.

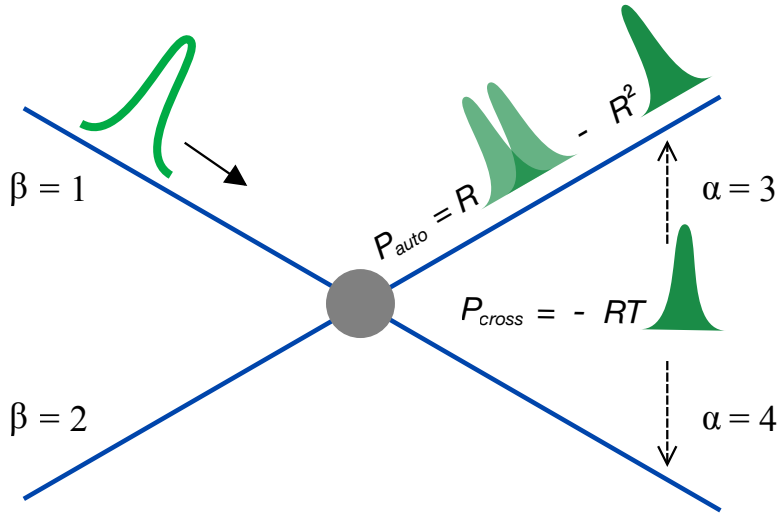

Figure 1. Shot noise, see Equation (10), of a single-electron wave packet injected on top of the Fermi sea consists of two parts: One is determined by the density profile of the wave packet, shown as a filled hump, and the other is determined by both the coherence of the wave packet, shown as a double hump, and the Fermi sea, shown as a blue line. While the former contributes to both auto-correlation noise, $\mathcal{P}_{auto}$, and cross-correlation noise, $\mathcal{P}_{cross}$, the latter contributes to $\mathcal{P}_{auto}$ only. The solid arrow indicates the wave packet in incoming channel $\beta = 1$, shown as an empty hump. The filled circle represents the wave splitter with reflection probability R and transmission probability $T = 1 - R$. The two dashed arrows point to the two outgoing leads $\alpha = 3$ and $\alpha = 4$.

Equation (1) is the main result of this work, which shows us that in the weak backscattering regime, the auto-correlation noise and cross-correlation noise are determined by essentially different quantities. One can say that they provide somehow complementary information. The cross-correlation noise is sensitive merely to the shape of a wave packet,

that is, to its duration in time, while the auto-correlation noise is rather sensitive to how different parts of the wave packet correlate with each other. Such correlations are related to the spread of the wave packet in energy, which is supported by the reasoning in [9] that only those particles whose energy exceeds the Fermi energy by more than $\hbar\omega$ contribute to the auto-correlation noise at the frequency ω.

Below, I use three known wave functions of particles injected into the Fermi sea by various electronic sources and calculate the corresponding auto- and cross-correlation noise in accordance with Equation (1). These results provide additional evidence of the duality of the information provided by both types of noise.

A Lorentzian voltage pulse, one per period, $eV(t) = 2\hbar\Gamma_\tau\left(t^2+\Gamma_\tau^2\right)^{-1}$, applied to the Fermi sea with energy μ and at zero temperature creates a single-electron wave packet [36,37], named a leviton [4]. This excitation should be understood in such a way that the voltage pulse shakes the Fermi sea and excites just a single electron on its surface [38]. The wave function of a leviton, $\Psi^L(t) = e^{-\frac{i}{\hbar}\mu t}\psi^L(t)$, has the following envelope function [39],

$$\psi^L(t) = \frac{1}{\sqrt{\pi\Gamma_\tau}}\frac{\Gamma_\tau}{t-i\Gamma_\tau}. \tag{4}$$

Here, the subscript τ indicates that Γ_τ is the half-width of the wave packet in time. I assume $\Gamma_\tau \ll \mathcal{T}_0$ to avoid overlap between the successive wave packets.

Using the above equation in Equation (1), I calculate

$$\mathcal{P}^{ex,L}_{auto}(\omega) = -\mathcal{P}^{L}_{cross}(\omega) \quad = \quad R\frac{e^2}{\mathcal{T}_0}e^{-|\omega|2\Gamma_\tau}. \tag{5}$$

The fact that the auto- and cross-correlation noise show the same frequency dependence is because there is only one time parameter in the problem, Γ_τ, which defines both the characteristic energy of the wave packet, $\hbar/(2\Gamma_\tau)$ [39], and the characteristic width in time of the wave packet, $2\Gamma_\tau$.

In the next example, the shape and the energy distribution are not related so tight and $\mathcal{P}^{ex}_{auto}(\omega)$ and $-\mathcal{P}_{cross}(\omega)$ become different.

Let us consider a quantum level of half-width δ filled with one electron and tunnel-coupled to a one-dimensional Fermi sea at zero temperature. The energy of a level raises at a constant rapidity c, and crosses the Fermi level at $t = 0$ when an electron is injected into the Fermi sea. Such regime of injection can be realized using the quantum capacitor [40–42]. The wave function of the injected electron was calculated in [43], $\Psi^c(t) = e^{-\frac{i}{\hbar}\mu t}\psi^c(t)$, with

$$\psi^{(c)}(t) \quad = \quad \frac{1}{\sqrt{\pi\Gamma_\tau}}\int_0^\infty dx e^{-x}e^{-ix\frac{t}{\Gamma_\tau}}e^{ix^2\frac{\tau_D}{\Gamma_\tau}}, \tag{6}$$

where $\Gamma_\tau = \delta/c$ is the crossing time, the time it takes for a raising widened quantum level to cross the Fermi level, $\tau_D = \hbar/(2\delta)$ is the dwell time, an average time spent an electron on a quantum level before escaping to the Fermi sea provided that such an escape is possible, that is, after the quantum level has risen above the Fermi level. Note that if $\tau_D \ll \Gamma_\tau$, then ψ^c, Equation (6), is essentially ψ^L, Equation (4). Notice, to get a stream of electrons we need a set of levels. Subsequent crossings occur with a delay of $\mathcal{T}_0 \gg \Gamma_\tau, \tau_D$. Now Equations (1) and (6) give us

$$\begin{aligned}\mathcal{P}^{ex,c}_{auto}(\omega) &= R\frac{e^2}{\mathcal{T}_0}e^{-|\omega|2\Gamma_\tau}, \\ \mathcal{P}^{c}_{cross}(\omega) &= -R\frac{e^2}{\mathcal{T}_0}\frac{e^{-|\omega|2\Gamma_\tau}}{1+(\omega\tau_D)^2}.\end{aligned} \tag{7}$$

For this model, the crossing time $2\Gamma_\tau$ is the only parameter that determines the energy distribution, the same as for the source of levitons [44]. This is why the auto-correlation noise is the same as in the first example.

However, the shape of the wave packet is different from that of a leviton. It is determined by both time parameters Γ_τ and τ_D. Namely, if the dwell time is comparable with the crossing time, $\tau_D \gtrsim \Gamma_\tau$, the density profile becomes larger than $2\Gamma_\tau$, asymmetric, and with some wavy structure developing at later times. All this leads to additional suppression of $\mathcal{N}(\omega)$ and $\mathcal{P}^c_{cross}(\omega)$ with increasing frequency compared to the first example. In the case when $\tau_D \gg \Gamma_\tau$, the dwell time, not the crossing time, determines how the cross-correlation noise decreases with frequency.

The connection between the auto-correlation noise and energy becomes even more transparent in the final example, where the dwell time is the only characteristic time.

The final (third) example is injection from a quantum dot with the equidistant ladder of levels, which is suddenly raised by one level spacing Δ at $t = 0$ [42,45]. The Fermi level is exactly between the two successive levels. The probability of tunneling between the dot and the Fermi sea is small. The wave function, $\Psi^\Delta(t) = e^{-\frac{i}{\hbar}\mu t}\psi^\Delta(t)$, has an envelope [35,46]

$$\psi^\Delta(t) \quad = \quad \theta(t)\frac{e^{-i\omega_0 t}}{\sqrt{\tau_D}}e^{-\frac{t}{2\tau_D}}. \tag{8}$$

Here, $\theta(t)$ is the Heaviside step function and $\hbar\omega_0 = \Delta/2$. Notice, in this case, the wave packet width is determined by the dwell time, while the energy of an injected electron is $\hbar\omega_0$, which is unrelated to τ_D.

For not too large frequencies, $\omega \ll \Delta/\hbar$, the straightforward calculations based on Equation (1) lead to the following result (see Appendix A for details):

$$\begin{aligned} \mathcal{P}^{ex,\Delta}_{auto}(\omega) &= R\frac{e^2}{\mathcal{T}_0}, \\ \mathcal{P}^{\Delta}_{cross}(\omega) &= -R\frac{e^2}{\mathcal{T}_0}\frac{1}{1+(\omega\tau_D)^2}. \end{aligned} \tag{9}$$

As the particles are injected far above the Fermi sea, $\Delta/2 \gg \hbar\omega$, all of them contribute to noise. As a result, there is no energy related suppression (for $\omega \ll \Delta/\hbar$ and $R \ll 1$). Therefore, the auto-correlation noise is independent on frequency. On the other hand, the density profile has a finite width, τ_D. Therefore, the cross-correlation noise gets suppressed at $\omega \geq \tau_D^{-1}$.

One more important conclusion can be drawn from Equation (1). In the case when a single-particle envelope wave function, ψ, is real-valued, for example, as for Majorana fermions [47,48], the corresponding contribution to the auto-correlation noise is identically zero in the weak backscattering regime. I emphasize that this conclusion applies to traveling single particles in the Fermi sea, and not to localized states.

For some injection protocols the auto-correlation noise is also zero for $R = 1$, see in [49].

Note that the charge conservation implies $\mathcal{P}^{ex}_{auto}(0) + \mathcal{P}_{cross}(0) = 0$, see Appendix B.3 [14]. This fact imposes some indirect constraint on the wave function of a single-electron wave packet that can be injected into a one-dimensional Fermi sea. In particular, no single particle with a real wave function can be injected in a clean manner, that is, without accompanying electron–hole pairs. Indeed, as Equation (1) predicts, the cross-correlation noise at zero frequency is not zero, $\mathcal{P}_{cross}(0) = -Re^2/\mathcal{T}_0 \neq 0$. While in the case of a real-valued wave function, the excess auto-correlation noise vanishes for any frequency, $\mathcal{P}^{ex}_{auto}(\omega) = 0$. To eliminate the apparent violation of charge conservation and ensure $\mathcal{P}^{ex}_{auto}(0) = -\mathcal{P}_{cross}(0) \neq 0$, we must assume that if such a particle is injected, then the additional excitations are unavoidable created. The example is a half-leviton [50], a particle

with a real wave function whose creation is accompanied by the creation of an electron–hole cloud.

The rest of the paper is structured as follows. In Section 2, within the framework of the Floquet scattering matrix approach, a connection is established between the correlation functions of the electrical current, the auto- and cross-correlation noise power, and the first-order correlation function of a periodic stream of electrons injected into a chiral Fermi sea. This relationship allows a detailed analysis of the similarities and differences between auto- and cross-correlation noise, which is illustrated in Section 3 using some examples. The conclusion is given in Section 4. Some technical details of calculations are presented in Appendices A–D.

2. Electrical Noise and Electron Correlation Function

In general, an external source is required to pass current through a conductor. The role of the source can be played, for example, by a constant or time-dependent voltage applied across a conductor; a time-dependent gate voltage, which changes the position of the quantum levels of electrons in a part of the conductor; etc. If the characteristics of the source are known, the current can be calculated. In the quantum coherent regime, when the current is carried by individual electrons, the characteristics of carriers, for example, their wave function, also can be calculated using the characteristics of the source. The measurements of electrical current and its fluctuations were already used to acquire information on quantum state of carriers [1,2,15]. Therefore, it is desirable to have a direct relation between the electrical and electron characteristics without explicit recursion to the characteristics of the source. Some efforts in this direction have already been made [44,50–52]. Below the fluctuations of an electrical current are expressed in terms of the wave functions, more precisely, in terms of the excess first-order correlation function [17,18,35,46] of electrons responsible for those fluctuations.

To be specific, here I am interested in a quantum coherent conductor connected via one-channel (chiral) leads [53] to several electron reservoirs in equilibrium. Some (or all) incoming leads are fed by external sources working periodically with period $\mathcal{T}_0$.

Below, I use the theory of non-interacting electrons. This is justified by the fact that such a theory has proved useful in describing the injection of single electrons [4,42], the results of quantum tomography of single electrons [1,2], and, in particular, the frequency-dependent noise [8,9] of interest here.

2.1. Frequency-Dependent Noise

The correlation function of currents, I_α, $I_{\alpha'}$, flowing in leads α and α' of a multi-terminal conductor are defined as follows [14]:

$$\mathcal{P}_{\alpha\alpha'}(\omega) = \int_0^{\mathcal{T}_0} \frac{dt}{\mathcal{T}_0} \int_{-\infty}^{\infty} d\tau e^{i\omega\tau} \left\{ \frac{\left\langle \hat{I}_\alpha(t+\tau)\hat{I}_{\alpha'}(t) + \hat{I}_{\alpha'}(t)\hat{I}_\alpha(t+\tau) \right\rangle}{2} - I_\alpha(t+\tau) I_{\alpha'}(t) \right\}, \tag{10}$$

where $\hat{I}_\alpha$ and $I_\alpha = \langle \hat{I}_\alpha \rangle$ are an operator in second quantization and a corresponding measurable for a current in the lead α; the angular brackets $\langle \dots \rangle$ denote the quantum statistical average; for a periodic drive, $\mathcal{T}_0$ is a period, for a non-periodic drive $\mathcal{T}_0 \to \infty$. Note the difference in the factor of 2 compared to the definition used in [14].

The current operator $\hat{I}_\alpha$ is expressed in terms of creation and annihilation operators $\hat{a}^\dagger_\alpha(E), \hat{a}_\alpha(E)$ of electrons with energy E incoming from the reservoir α and operators $\hat{b}^\dagger_\alpha(E), \hat{b}_\alpha(E)$ of electrons with energy E scattered into the reservoir α [54]. In the wide band limit, that is, when the relevant energy scales, such as a voltage applied, a temperature, the energy quantum $\hbar\Omega$ with $\Omega = 2\pi/\mathcal{T}_0$, etc., are all small compared to the Fermi energy μ_α, the current operator reads [55],

$$\hat{I}_\alpha(t) = \frac{e}{h} \iint dE dE' e^{i\frac{E-E'}{\hbar}t} \left\{ \hat{b}^\dagger_\alpha(E)\hat{b}_\alpha(E') - \hat{a}^\dagger_\alpha(E)\hat{a}_\alpha(E') \right\}. \tag{11}$$

In the case of a periodically driven conductor, the operators $\hat{b}_\alpha$ are related to various operators $\hat{a}_\alpha$ via the elements of the unitary Floquet scattering matrix S_F [56],

$$\hat{b}_\alpha(E) \;=\; \sum_\beta \sum_{n=-\infty}^{\infty} S_{F,\alpha\beta}(E, E_n)\hat{a}_\beta(E_n), \tag{12}$$

where the short notation $E_n = E + n\hbar\Omega$ is introduced. Charge conservation requires the scattering matrix to be unitary, which means

$$\begin{aligned} \sum_\gamma \sum_{n=-\infty}^{\infty} S^*_{F,\gamma\alpha}(E_n, E_m)S_{F,\gamma\beta}(E_n, E) &= \delta_{\alpha\beta}\delta_{m,0}, \\ \sum_\gamma \sum_{n=-\infty}^{\infty} S^*_{F,\alpha\gamma}(E_m, E_n)S_{F,\beta\gamma}(E, E_n) &= \delta_{\alpha\beta}\delta_{m,0}, \end{aligned} \tag{13}$$

where $\delta_{n,0}$ is the Kronecker delta.

Equation (12) allows to express the quantum-statistical average of the product of b-operators in terms of that of a-operators. Because the reservoirs are in equilibrium, the latter average is known. In the case of reservoirs of non-interacting electrons forming the Fermi sea, we have $\left\langle \hat{a}^\dagger_\beta(E)\hat{a}_\beta(E')\right\rangle = f_\beta(E)\delta(E-E')$, where $f_\beta(E)$ is the Fermi distribution function with temperature θ_β and chemical potential μ_β, and $\delta(E-E')$ is the Dirac delta.

2×2 Circuit

Our aim is to compare auto- and cross-correlation noise. The minimal circuit that allows cross-correlation noise is an electronic wave splitter, a quantum point contact (QPC) with two incoming, $\beta = 1, 2$, and two outgoing, $\alpha = 3, 4$, channels, see Figure 1.

Below, I am interested in current fluctuations in outgoing channels, that is, $\alpha, \alpha' = 3, 4$ in Equation (10). For this case, the general equation for noise within the Floquet scattering matrix approach [57,58] gives us

$$\begin{aligned} \mathcal{P}_{33}(\omega) = \frac{e^2}{h}\int dE \Big\{ F_{33}(E, E+\hbar\omega) + \sum_{n,m,q=-\infty}^{\infty} \sum_{\delta=1}^{2}\sum_{\gamma=1}^{2} F_{\gamma\delta}(E_q+\hbar\omega, E) \\ \times S^*_{F,3\delta}(E_n, E)S_{F,3\delta}(E_m, E)S^*_{F,3\gamma}(E_m+\hbar\omega, E_q+\hbar\omega)S_{F,3\gamma}(E_n+\hbar\omega, E_q+\hbar\omega)\Big\}, \end{aligned} \tag{14a}$$

and

$$\begin{aligned} \mathcal{P}_{34}(\omega) = \frac{e^2}{h}\int dE \sum_{n,m,q=-\infty}^{\infty} \sum_{\delta=1}^{2}\sum_{\gamma=1}^{2} F_{\gamma\delta}(E_q+\hbar\omega, E)S^*_{F,3\delta}(E_n, E)S_{F,4\delta}(E_m, E) \\ \times S^*_{F,4\gamma}(E_m+\hbar\omega, E_q+\hbar\omega)S_{F,3\gamma}(E_n+\hbar\omega, E_q+\hbar\omega), \end{aligned} \tag{14b}$$

with

$$F_{\gamma\delta}(E_1, E) = \frac{f_\gamma(E_1) + f_\delta(E)}{2} - f_\gamma(E_1)f_\delta(E). \tag{15}$$

Let us also introduce excess noise, that is, an increase in noise due to the source, which is defined as the following difference:

$$\mathcal{P}^{ex}_{\alpha\alpha'}(\omega) = \mathcal{P}_{\alpha\alpha'}(\omega) - \mathcal{P}^{off}_{\alpha\alpha'}(\omega), \tag{16}$$

where the upper index off indicates that the source is switched off.

I suppose a unitary 2×2 scattering matrix of the QPC to be energy-independent,

$$S^{QPC} = \begin{pmatrix} \sqrt{R} & i\sqrt{T} \\ i\sqrt{T} & \sqrt{R} \end{pmatrix}, \tag{17}$$

a real number $0 \leq R \leq 1$ is the reflection probability, the transmission probability $T = 1 - R$. We need an energy independent S^{QPC} in order to use noise to get information on injected wave packets only. If the properties of the electronic circuit that connects the incoming and outgoing channels do depend on energy, the outgoing signal also carries nontrivial information about the circuit [59].

In addition, for the sake of simplicity, I suppose that the periodic source is present only in the incoming channel $\beta = 1$. This source characterized by the Floquet scattering amplitude, which is a matrix in an energy space with elements $S_F(E, E_n)$. The results presented below can be directly generalized to the case when another source is added in the second incoming channel, see Appendix B.4.

For the circuit with single source and single QPC, the elements of the total Floquet scattering matrix are represented as follows:

$$\begin{aligned} S_{F,31}(E, E_n) &= \sqrt{R} S_F(E, E_n), \\ S_{F,41}(E, E_n) &= i\sqrt{T} S_F(E, E_n), \\ S_{F,32}(E, E_n) &= i\sqrt{T}\delta_{n,0}, \\ S_{F,42}(E, E_n) &= \sqrt{R}\delta_{n,0}. \end{aligned} \tag{18}$$

All other elements are zero.

2.2. First-Order Correlation Function

To characterize a quantum state injected by the source into a ballistic one-dimensional electronic waveguide, I use the first-order correlation function, $\mathcal{G}^{(1)}$. This function is defined as a quantum statistical average of the product of two field operators for electrons calculated in the electronic wave-guide β just after the source, $\mathcal{G}^{(1)}_{\beta}(t_1; t_2) = \left\langle \hat{\Psi}^{\dagger}_{\beta}(t_1)\hat{\Psi}_{\beta}(t_2) \right\rangle$ [17]. Strictly speaking, this object is a 2×2 matrix in the spin space. However, here I consider the spin-polarized case and suppress the spin index.

When the source is placed in lead $\beta = 1$ and is characterized by the Floquet scattering amplitude, $S_F(E_n, E)$, the corresponding correlation function is calculated as follows [51]:

$$v_{\mu}\mathcal{G}^{(1)}_1(t + \tau; t) = \frac{1}{h}\int dE f_1(E) e^{\frac{i}{\hbar}E\tau} \sum_{n,m=-\infty}^{\infty} e^{i\Omega n\tau} e^{i\Omega(n-m)t} S^{*}_F(E_n, E) S_F(E_m, E). \tag{19}$$

Here, v_{μ} is a velocity of electrons at the Fermi level, which is originated from the density of states being energy independent in the wide band limit used here.

When the source is switched off, $S_F(E_n, E) = \delta_{n,0}$, the above equation is reduced to the correlation function of the Fermi sea in equilibrium, which depends on the difference of times rather than on two times separately. I denote the equilibrium correlation function by the complementary subscript 0 and obtain for lead β, $\left[\mathcal{G}^{(1)}_{0,\beta}(\tau) \equiv \mathcal{G}^{(1)}_{0,\beta}(t + \tau; t)\right]$

$$v_{\mu}\mathcal{G}^{(1)}_{0,\beta}(\tau) = \frac{1}{h}\int dE f_{\beta}(E) e^{i\frac{E}{\hbar}\tau} = \frac{e^{i\tau\frac{\mu_{\beta}}{\hbar}}}{2\pi i} \frac{1/\tau_{\theta_{\beta}}}{\sinh\left(\tau/\tau_{\theta_{\beta}}\right)}. \tag{20}$$

Here, $\tau_{\theta_{\beta}} = \hbar/(\pi k_B \theta_{\beta})$ is the thermal coherence time for the reservoir, where the lead β is attached to.

The difference of correlation functions with the source being on and off is the excess correlation function, which characterizes what is injected by the source into an electron waveguide $\beta = 1$ [18],

$$G_1^{(1)}(t_1;t_2) \quad = \quad \mathcal{G}_1^{(1)}(t_1;t_2) - \mathcal{G}_{0,1}^{(1)}(t_1 - t_2). \tag{21}$$

In the case when the source injects a single electron with wave function $\Psi(t)$ per period, the excess correlation function during that period takes on a very simple form, $G_1^{(1)}(t_1;t_2) = \Psi^*(t_1)\Psi(t_2)$. In the case of injection of N electrons, $G_1^{(1)}(t_1;t_2) = \sum_{j=1}^{N} \Psi_j^*(t_1)\Psi_j(t_2)$ [20].

2.3. Noise Power in Terms of $\mathcal{G}^{(1)}$

For non-interacting electrons, the correlation function $\mathcal{G}^{(1)}$ contains complete information about the system of electrons. In particular, all measurables can be expressed in terms of correlation function, see, e.g., in [51] for some examples. Such expressions are notably useful when transport is due to only a few electrons per period.

Here, I express the excess noise in terms of $G^{(1)}$ in the case when all incoming channels have the same temperature $\theta_\beta = \theta$ and Fermi energy $\mu_\beta = \mu$. Therefore, the equilibrium electronic correlation functions are the same, $\mathcal{G}_{0,\beta}^{(1)} = \mathcal{G}_0^{(1)}$. For more general case and for details of calculations, see Appendix B.

First, let us substitute Equations (15) and (18) into Equation (14) and calculate the excess noise, Equation (16). As a result, I find for the auto-correlation noise (see Equation (A20)),

$$\mathcal{P}_{33}^{ex}(\omega) \quad = \quad e^2 v_\mu^2 \int_0^{\mathcal{T}_0} \frac{dt}{\mathcal{T}_0} \int_{-\infty}^{\infty} d\tau e^{i\omega\tau} \Big\{ -R^2 \Big| G_1^{(1)}(t+\tau;t) \Big|^2 - 2R\,\mathrm{Re} G_1^{(1)}(t+\tau;t) \mathcal{G}_0^{(1)*}(\tau) \Big\}, \tag{22a}$$

and for the cross-correlation noise (see Equation (A24)),

$$\mathcal{P}_{34}(\omega) \quad = \quad -RTe^2 v_\mu^2 \int_0^{\mathcal{T}_0} \frac{dt}{\mathcal{T}_0} \int_{-\infty}^{\infty} d\tau e^{i\omega\tau} \Big| G_1^{(1)}(t+\tau;t) \Big|^2. \tag{22b}$$

The above equations are the central result of this work.

Notice that when all reservoirs are in the same conditions, cross-correlation noise disappears when the source is turned off. This is why the superscript ex is omitted.

The important difference between auto- and cross-correlation noise (Equations (22a) and (22b)) is that the latter is determined solely by what is injected by the source, while the former in addition depends explicitly on the properties of the Fermi sea.

The part of the noise that is determined by $\left| G_1^{(1)} \right|^2$ depends on the possible quantum exchange [14] between the injected electrons. At zero temperature and when electrons are injected one at a time without overlapping, this part of the noise is reduced to the product of currents in Equation (10). In the wide band approximation used here, the electric current is proportional to the density profile of the wave packet, hence Equation (1), the second line.

In contrast, the part of the noise that is determined by the product of $G_1^{(1)}$ and $\mathcal{G}_0^{(1)}$ takes into account the quantum exchange of an injected electron and electrons of the Fermi sea. Such an exchange does not contribute to cross-correlation noise, unless the two incoming Fermi seas are different, see Equation (A23).

The formal difference between the auto- and cross-correlation noise becomes especially pronounced in the weak back-scattering regime, $R \ll 1$, when we can discard the terms $\sim R^2$ in Equation (22) and get the following,

$$\begin{aligned} \mathcal{P}_{33}^{ex}(\omega) &= -Re^2 v_\mu^2 \int_0^{\mathcal{T}_0} \frac{dt}{\mathcal{T}_0} \int_{-\infty}^{\infty} d\tau e^{i\omega\tau} 2\mathrm{Re} G_1^{(1)}(t+\tau;t) \mathcal{G}_0^{(1)*}(\tau), \\ \mathcal{P}_{34}(\omega) &= -Re^2 v_\mu^2 \int_0^{\mathcal{T}_0} \frac{dt}{\mathcal{T}_0} \int_{-\infty}^{\infty} d\tau e^{i\omega\tau} \left| G_1^{(1)}(t+\tau;t) \right|^2. \end{aligned} \tag{23}$$

Notice that using Equation (20) for $\mathcal{G}_0^{(1)}$ at zero temperature, $\theta = 0 \Rightarrow \tau_\theta \to \infty$, and for a single-particle injection, $G^{(1)}(t+\tau;t) = e^{i\frac{\mu}{\hbar}\tau}\psi^*(t+\tau)\psi(t)$, we arrive at Equation (1) with $\mathcal{P}_{auto}^{ex} = \mathcal{P}_{33}^{ex}$ and $\mathcal{P}_{cross} = \mathcal{P}_{34}$, where integration over t is extended to infinity, as the duration of the wave packet is much less than the period $\mathcal{T}_0$.

3. Examples

In this section, I will consider two examples: one when auto- and cross-correlation noise are perfectly anti-correlated at any frequency, and the other when they can be different. The corresponding equations are valid for arbitrary R, and not only for $R \ll 1$, as in the examples given in the introductory section.

3.1. Energy-Independent Source

In the case when the properties of the source do not change on the scale of the energy of the injected particles, the corresponding Floquet scattering amplitude can be represented as a Fourier coefficient of a certain energy-independent scattering amplitude, $S_F(E_n, E) = \int_0^{\mathcal{T}_0} \frac{dt}{\mathcal{T}_0} e^{2\pi i n \frac{t}{\mathcal{T}_0}} S(t)$ [46,56]. In a one-dimensional case, unitarity implies that $S(t)$ is a pure phase factor, that is, $|S(t)|^2 = 1$. For example, if a voltage $V(t)$ plays the role of a source, then this phase factor reads $S(t) = \exp\left(i\frac{e}{\hbar}\int^t dt' V(t')\right)$.

In such a case, Equation (19) gives us $\mathcal{G}_1^{(1)}(t_1;t_2) = S^*(t_1)S(t_2)\mathcal{G}_{0,1}^{(1)}(t_1 - t_2)$. Note that $\mathcal{G}_{0,1}^{(1)}$ describes the Fermi sea in equilibrium at temperature θ_1. Using this result in Equation (22), and taking into account that

$$G_1^{(1)}(t_1;t_2) = \{S^*(t_1)S(t_2) - 1\}\mathcal{G}_{0,1}^{(1)}(t_1 - t_2), \tag{24}$$

we find that the excess auto- and cross-correlation noise are perfectly anti-correlated at any frequency,

$$\mathcal{P}_{33}^{ex}(\omega) + \mathcal{P}_{34}(\omega) = 0, \tag{25}$$

not only at zero frequency, $\omega = 0$, as the charge conservation requires [14]. An example was shown in Equation (5).

For $R = 1$, when cross-correlation noise does not exist, that is, formally $\mathcal{P}_{34} = 0$, the above equation tells us that whatever emitted by the source under consideration is silent on any frequency, the excess auto-correlation noise is zero, $\mathcal{P}_{33}^{ex}(\omega) = 0$. In particular, any voltage applied to a ballistic channel produces no excess noise at any frequency. Note that for a generic source injecting electrons into a ballistic waveguide, a similar conclusion can be drawn for noise only at zero frequency, see Equation (A25). Note that in the case of $R = 1$, zero excess auto-correlation noise tells us nothing about the number of excited particle–hole pairs. In order to count the number of excitations, we need a wave-splitter with $R < 1$.

Some general conclusions can be made regarding the effect of temperature on noise. Indeed, Equations (20) and (24) allow us to relate the excess correlation function at zero (the extra subscript 0) and non-zero (the extra subscript θ) temperatures as follows:

$$G^{(1)}_{1,\theta}(t+\tau;t) = \frac{\tau/\tau_\theta}{\sinh(\tau/\tau_\theta)}\, G^{(1)}_{1,0}(t+\tau;t). \tag{26}$$

Then, I use the above equation in Equations (22a) and (22b), utilize the inverse Fourier transformation with respect to ω, and express the noise at temperature θ, $\mathcal{P}^{ex}_\theta$, in terms of the noise at zero temperature, $\mathcal{P}^{ex}_0$, as follows,

$$\mathcal{P}^{ex}_\theta(\omega) \;=\; \int\limits_{-\infty}^{\infty} d\tau e^{i\omega\tau}\left(\frac{\tau/\tau_\theta}{\sinh(\tau/\tau_\theta)}\right)^2 \int\limits_{-\infty}^{\infty} \frac{d\omega'}{2\pi} e^{-i\omega'\tau}\mathcal{P}^{ex}_0(\omega'). \tag{27}$$

Here, I introduce $\mathcal{P}^{ex} \equiv \mathcal{P}^{ex}_{33} = -\mathcal{P}_{34}$ according to Equation (25).

3.2. Injection from a Quantum Level Raising at a Constant Rapidity

Now, let us consider a single-electron injection from a source, whose properties depend on energy. The corresponding scattering amplitude and the wave function of the injected electron were discussed in [43] at zero temperature and in [60] at nonzero temperatures. In this case, the auto- and cross-correlation noises do not stick together unless at zero frequency.

At zero temperature, the excess correlation function is $v_\mu G^{(1)}_1(t+\tau;t) = e^{i\frac{\mu}{\hbar}\tau}\psi^{(c)*}(t+\tau)\psi^{(c)}(t)$, where $\psi^{(c)}$ is shown in Equation (6). Using this equation in Equations (22a) and (22b) and assuming that the width of the wave packet is small compared to the period, $\max(\Gamma_\tau, \tau_D) \ll \mathcal{T}_0$, I find (see Appendix C for details),

$$\begin{aligned}
\mathcal{P}^{ex}_{33}(\omega) &= R\frac{e^2}{\mathcal{T}_0}\frac{T+(\omega\tau_D)^2}{1+(\omega\tau_D)^2}e^{-|\omega|2\Gamma_\tau},\\
\mathcal{P}_{34}(\omega) &= -R\frac{e^2}{\mathcal{T}_0}\frac{T}{1+(\omega\tau_D)^2}e^{-|\omega|2\Gamma_\tau}.
\end{aligned} \tag{28}$$

At $R \ll 1$ ($T \approx 1$), Equation (7) is reproduced.

The above equations are illustrated in Figure 2 in the case of $2\Gamma_\tau \ll \tau_D$, when the difference between them is most pronounced. As I have already discussed in the introduction after Equation (7), the excess auto-correlation noise and the cross-correlation noise demonstrate significantly different dependencies on frequency. The cross-correlation noise (its absolute value) decreases monotonically with frequency, see Figure 2, a red dashed line. In contrast, the excess auto-correlation noise is non-monotonically dependent on frequency, which is a manifestation of the existence of two contributions. The first contribution, which is responsible for the quadratic increase at low frequencies, is similar to the cross-correlation noise, compare the first term in Equations (22a) and (22b), while the second contribution is different. This contribution dominates in the limit of $T \to 1$ and at high frequencies, see a black solid line in Figure 2.

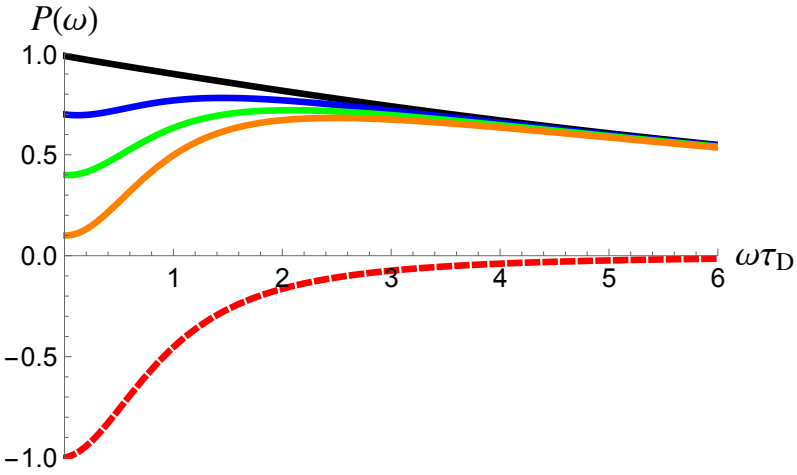

Figure 2. The excess auto- (solid lines) and cross-correlation (a red dashed line) noise is shown as a function of the frequency ω at zero temperature, see Equation (28). The cross-correlation noise, $P \equiv \mathcal{P}_{34}$, is given in units of $RTe^2/\mathcal{T}_0$. The excess auto-correlation noise, $P \equiv \mathcal{P}^{ex}_{33}$, is given in units of $Re^2/\mathcal{T}_0$ for $T = 0.999$ (a black line), $T = 0.7$ (a blue line), $T = 0.4$ (a green line), and $T = 0.1$ (an orange line). The parameter $2\Gamma_\tau/\tau_D = 0.1$.

At non-zero temperature, $\theta > 0$, auto- and cross-correlation noise is modified by the same factor, $\mathcal{P}^{ex}_{33,\theta}(\omega) = \eta(\omega,\theta)\mathcal{P}^{ex}_{33}(\omega)$ and $\mathcal{P}_{34,\theta}(\omega) = \eta(\omega,\theta)\mathcal{P}_{34}(\omega)$ (see Appendix D for details), where

$$\eta(\omega,\theta) = e^{|\omega|2\Gamma_\tau} \int_{-\infty}^{\infty} \frac{dx}{\pi} \frac{e^{ix\omega 2\Gamma_\tau}}{x^2+1} \left(\frac{x2\Gamma_\tau/\tau_\theta}{\sinh(x2\Gamma_\tau/\tau_\theta)} \right)^2. \tag{29}$$

The thermal coherence time τ_θ is defined after Equation (20).

Interestingly, the above equation is independent of the dwell time $\tau_D = \hbar/(2\Gamma_\tau c)$, where c is a rapidity, see Equation (6). Therefore, the same factor $\eta(\omega,\theta)$ applies for the case of $\tau_D = 0$, which is the case for the source of levitons of half-width Γ_τ. However, this analogy is not complete.

Namely, for the case of levitons, the noise at non-zero temperatures can be expressed directly in terms of the noise at zero temperature, see Equation (27). On the contrary, for the case of electrons emitted from the quantum level, this is generally not the case due to factors that depend on $\omega\tau_D$. Yet, in the weak backscattering regime, $R \ll 1$, the auto-correlation noise obeys Equation (27), because it has no such factors, see Equation (7).

The temperature-dependent factor $\eta(\omega,\theta)$, Equation (29), is shown in Figure 3 for several frequencies ω. Remarkably, the maximum occurs at $\omega\tau_\theta \sim 1$, which is independent of properties of the source. The non-monotonic temperature behavior at non-zero frequencies is due to two counteracting effects, both due to the fact that the quantum state of electrons injected at non-zero temperatures is a mixed quantum state [51].

The first effect, which leads to noise suppression, comes from the fact that each component of a mixed state is scattered independently at the wave splitter. As a result, the effect of charge quantization becomes less pronounced, and shot noise decreases with increasing temperature. At $\theta \gg \theta_0$, where the characteristic temperature, θ^*, is determined by the energy of an injected electron, $k_B\theta_0 = \hbar/(2\pi\Gamma_\tau)$, the shot noise decays as θ_0/θ [61].

Suppression of a zero-frequency shot noise with temperature has been reported in [3,7,62,63]. For the source of levitons, this effect was predicted in [19].

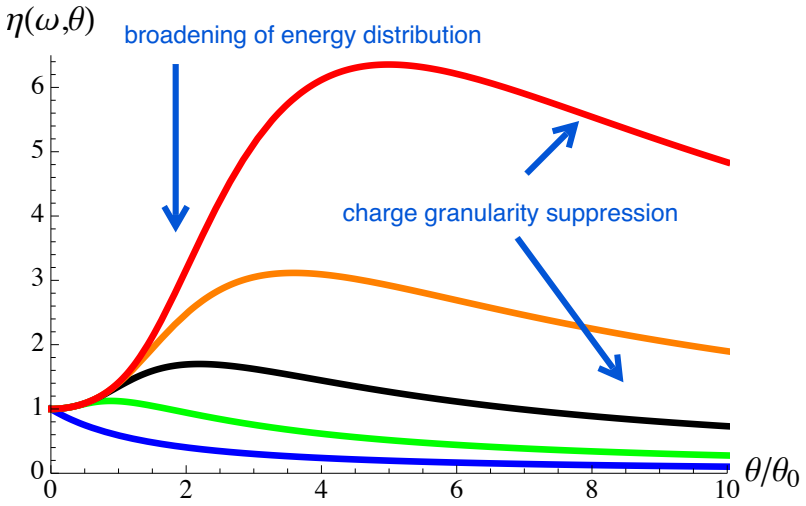

Figure 3. The factor $\eta(\omega,\theta)$, Equation (29), is shown as a function of the temperature θ for $\omega = n/(2\Gamma_\tau)$ with $n = 0$ (blue), $n = 1$ (green), $n = 2$ (black), $n = 3$ (orange), and $n = 4$ (red). The parameter θ_0 is such a temperature when the thermal coherence length is equal to the width of the wave packet: $\theta_0 = \hbar/(\pi k_B 2\Gamma_\tau)$.

The second effect, leading to an increase in noise, is associated with an effective broadening of the energy distribution of injected particles due to the broadening of the probability density of the components of the mixed state with increasing temperature, $p(\epsilon) = -\partial f_1(\epsilon)/\partial\epsilon$, see Equation (A40). As a result, the injected particle is more likely to be able to emit energy $\hbar\omega$ in order to contribute to noise at frequency ω [9]. This increase reaches saturation at $4k_B\theta \sim \hbar\omega$, which leads to the maxima in Figure 3.

4. Conclusions

The finite-frequency fluctuations of an electric current in multi-terminal conductors were analyzed at zero as well as non-zero temperatures. The focus was on the quantum coherent regime, when the current is carried by non-overlapping single-particle wave packets periodically injected into a unidirectional, chiral wave guide.

To highlight similarities and differences between auto- and cross-correlation noise, the fluctuations of an electric current were expressed in terms of the wave functions of injected electrons, bypassing the use of explicit source characteristics. Two contributions to shot noise have been identified. The first, which depends on the possible quantum exchange between the injected electrons, determines the cross-correlation noise and part of the auto-correlation noise. In the case of single-particle injection at zero temperature, this part is determined by the density profile of the injected wave packets. The second contribution, which depends on the quantum exchange of an injected electron and electrons of the Fermi sea, contributes only to the auto-correlation noise. This part is determined by the coherence of the injected wave packets multiplied by the coherence of the Fermi sea.

At zero frequency, the charge conservation tightly links both contributions to shot noise. Such a connection allows us to make some general conclusions related to the properties of excitations that can be injected/created in the Fermi sea. In particular, no excitations with a real wave function can be created in the Fermi sea without accompanying electron–hole pairs, which follows from the fact that otherwise Equation (1) would be incompatible with the conservation of charge [14]. At non-zero frequencies, the two contributions in question are generally different. They can be addressed separately by measuring both auto- and cross-correlation noise in the weak backscattering regime, $R \ll 1$.

For several experimentally available single-electron sources for which the wave function was calculated, I calculated and compared auto- and cross-correlation noise. For the family of so-called energy-independent sources, the source of leviton [4] is an example, the contribution related to the density profile and the contribution related to the coherence

of the wave packet turn out to be the same, see Equation (5). Therefore, the auto- and cross-correlation noises are the same (up to the minus sign) at any frequency, not only at zero frequency as the charge conservation requires, see Equation (25). For another source, which relies on tunneling [42], the two contributions are manifestly different, see Equations (7) and (9) for different working regimes of the source.

I analyzed the effect of temperature on shot noise in the case when electrons are injected on top of the Fermi. It turns out that temperature affects both contributions equally, see Equation (29) for the temperature-dependent factor. As one of the contributions to shot noise depends on the quantum state of electrons in the Fermi sea, I conclude that temperature affects the quantum state of both the electrons in the Fermi sea and the injected electrons in the same way. Namely, a pure state at zero temperature becomes a mixed state at non-zero temperatures [51]. At zero frequency, changing the quantum state from pure to mixed leads to noise suppression, while at non-zero frequencies, the temperature dependence of noise is non-monotonic, see Figure 3. The temperature-dependent factor peaks when the thermal coherence time becomes of the order of the inverse of the frequency at which the noise is measured. Importantly, the position of this maximum does not depend on the properties of the sources of electrons under consideration.

Funding: This research was funded by the Ministry of Education and Science of Ukraine, project No. 0119U002565.

Acknowledgments: I acknowledge the warm hospitality and support of Tel Aviv University. I am grateful to Pascal Degiovanni for stimulating discussions.

Conflicts of Interest: The author declares no conflict of interest.

Appendix A. Auto-Correlation Noise from Equation (9)

After substituting Equation (8) into Equation (1), the first line, I get

$$\mathcal{P}^{ex}_{auto}(\omega) = R\frac{e^2}{\mathcal{T}_0}\int_0^\infty \frac{dt}{\tau_D}\int_{-t}^\infty d\tau e^{i\omega\tau}\frac{\sin(\omega_0\tau)}{\pi\tau}e^{-\frac{t+\tau/2}{\tau_D}}. \tag{A1}$$

To integrate with respect to t, I split the integration area into two and interchange the order of integration,

$$\int_0^\infty dt\int_{-t}^\infty d\tau = \int_0^\infty d\tau\int_0^\infty dt + \int_{-\infty}^0 d\tau\int_{-\tau}^\infty dt.$$

Then, I have

$$\begin{aligned}\mathcal{P}^{ex}_{auto}(\omega) &= R\frac{e^2}{\mathcal{T}_0}\eta(\omega), \\ \eta(\omega) &= \int_0^\infty d\tau\cos(\omega\tau)e^{-\frac{\tau}{2\tau_D}}\frac{2\sin(\omega_0\tau)}{\pi\tau}.\end{aligned} \tag{A2}$$

The suppression factor $\eta(\omega)$ is shown in Figure A1.

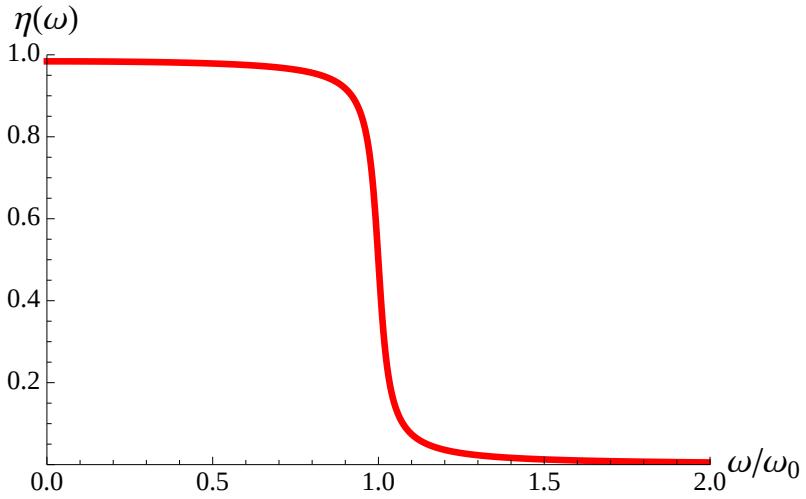

Figure A1. A frequency-dependent suppression factor $\eta(\omega)$, Equation (A2). The frequency ω is given in units of $\omega_0 = \Delta/(2\hbar)$, see Equation (8). The product $\omega_0\tau_D = 20$.

Let us first consider the case of $\omega = 0$, when

$$\eta(0) \quad = \quad \int_0^\infty d\tau e^{-\frac{\tau}{2\tau_D}} \frac{2\sin(\omega_0\tau)}{\pi\tau}. \tag{A3}$$

The integrand in the above equation has two factors, exponentially decaying and oscillating. The wave function ψ^Δ, Equation (8), was calculated in the limit of $\omega_0\tau_D \gg 1$ [35,46]. Therefore, the period of oscillations is much smaller then the time of decay. Therefore, namely, the fast oscillating factor determines an integral. The other, slowly decaying term can be calculated merely at $\tau = 0$. Thus, by using a textbook integral

$$\int_0^\infty d\tau \frac{\sin(\omega_0\tau)}{\tau} = \frac{\pi}{2},$$

I arrive at $\eta(0) = 1$.

For non-zero frequencies, I represent the factor $\eta(\omega)$ as follows:

$$\eta(\omega) \quad = \quad \int_0^\infty d\tau e^{-\frac{\tau}{2\tau_D}} \frac{\sin([\omega_0+\omega]\tau) + \sin([\omega_0-\omega]\tau)}{\pi\tau}. \tag{A4}$$

At small frequencies, $\omega \ll \omega_0$, I can neglect ω compared to ω_0, both sinuses becomes the same, and I recover $\eta(\omega \ll \omega_0) = \eta(0) = 1$. With this result, I reproduce Equation (9), the first line.

At $\omega = \omega_0$, the second sinus nullifies, and the result is halved, $\eta(\omega_0) = 0.5$. At higher frequencies, $\omega > \omega_0$, the two sinuses contribute the same, but with opposite sign, and the noise gets suppressed, $\eta(\omega) = 0$. The transition from one to zero happens to occur within the region of order τ_D^{-1} near $\omega = \omega_0$ (that is, near $\hbar\omega = \Delta/2$) in full agreement with the previous findings [9,64]. Here, I demonstrated that the wave function $\psi^\Delta(t)$, Equation (8), carries information about this noise suppression effect.

The calculations leading from Equation (1), the second line to Equation (9), and the second line with the wave function from Equation (8) are rather straightforward. Importantly, the cross-correlation noise gets suppressed at much smaller frequencies of order $\tau_D^{-1} \ll \omega_0$.

Note that Equation (9) was calculated for the case of weak scattering into the detector, $R \ll 1$. In contrast, in the opposite limiting case, $R = 1$, according to Equation (22a), the autocorrelation noise, the quantum jitter noise [8], is given by the combination of two

contributions to noise. As a result, it becomes suppressed not only at large frequencies, $\omega > \omega_0$, but also at small frequencies: $\mathcal{P}^{ex}_{33}(0 < \omega \ll \omega_0)\big|_{R=1} = \frac{e^2}{T_0}\frac{(\omega\tau_D)^2}{1+(\omega\tau_D)^2}$.

Appendix B. Relation between an Electrical Noise and an Electron Correlation Function

Here, I generalize the results of Section 2.3 to the case when the input channels have different temperatures and Fermi energies. For this, it is convenient to separate the terms linear and bilinear in the Fermi functions f_1 and f_2 in Equation (14a) and (14b) . I will distinguish such terms via the upper index l and b, respectively,

$$\begin{aligned}\mathcal{P}_{33}(\omega) &= \frac{e^2}{h}\int dE F_{33}(E, E+\hbar\omega) + \mathcal{P}^l_{33}(\omega) + \mathcal{P}^b_{33}(\omega),\\ \mathcal{P}_{34}(\omega) &= \mathcal{P}^l_{34}(\omega) + \mathcal{P}^b_{34}(\omega).\end{aligned} \tag{A5}$$

Appendix B.1. Auto-Correlation Nose

Let us first consider $\mathcal{P}_{33}$. Substituting Equation (18) into Equation (14a) and (14b), I find

$$\begin{aligned}\mathcal{P}_{33}(\omega) = \frac{e^2}{h}\int dE\Big\{F_{33}(E, E+\hbar\omega) + \sum_{n,m,q=-\infty}^{\infty}\\ R^2 f_{11}(E_q+\hbar\omega, E)S^*_F(E_n, E)S_F(E_m, E)S^*_F(E_m+\hbar\omega, E_q+\hbar\omega)S_F(E_n+\hbar\omega, E_q+\hbar\omega)\\ +TRf_{12}(E_q+\hbar\omega, E)\delta_{n0}\delta_{m0}S^*_F(E_m+\hbar\omega, E_q+\hbar\omega)S_F(E_n+\hbar\omega, E_q+\hbar\omega)\\ +RTf_{21}(E_q+\hbar\omega, E)S^*_F(E_n, E)S_F(E_m, E)\delta_{nq}\delta_{mq} + T^2 f_{22}(E_q+\hbar\omega, E)\delta_{n0}\delta_{m0}\delta_{nq}\delta_{mq}\Big\}.\end{aligned} \tag{A6}$$

Then, I use Equation (15) and calculate a linear in Fermi functions f_1 and f_2 part,

$$\mathcal{P}^l_{33}(\omega) = \frac{e^2}{2h}\int dE\Big\{Rf_1(E) + Rf_1(E+\hbar\omega) + Tf_2(E) + Tf_2(E+\hbar\omega)\Big\}. \tag{A7}$$

In the course of calculations, I utilized unitarity of the Floquet scattering matrix, see Equation (13). For a single-channel S_F, unitarity implies the following:

$$\begin{aligned}\sum_{n=-\infty}^{\infty} S^*_F(E_n, E_m)S_F(E_n, E) = \delta_{m,0},\\ \sum_{n=-\infty}^{\infty} S^*_F(E_m, E_n)S_F(E, E_n) = \delta_{m,0}.\end{aligned} \tag{A8}$$

As an example, let us consider the very first term we need to calculate,

$$\begin{aligned}\frac{e^2}{2h}\int dE \sum_{n,m,q=-\infty}^{\infty} R^2 f_1(E_q+\hbar\omega)S^*_F(E_n, E)S_F(E_m, E)\\ \times S^*_F(E_m+\hbar\omega, E_q+\hbar\omega)S_F(E_n+\hbar\omega, E_q+\hbar\omega).\end{aligned}$$

To simplify it, I shift $E_q \to E$ under integration over energy and shift $q \to -q$, $n-q \to n$, $m-q \to m$ under the corresponding sums,

$$\begin{aligned}\frac{e^2}{2h}\int dE \sum_{n,m,q=-\infty}^{\infty} R^2 f_1(E+\hbar\omega)S^*_F(E_n, E_q)S_F(E_m, E_q)\\ \times S^*_F(E_m+\hbar\omega, E+\hbar\omega)S_F(E_n+\hbar\omega, E+\hbar\omega).\end{aligned}$$

Then, the sum over q gives us $\sum_q S_F^*(E_n, E_q)S_F(E_m, E_q) = \delta_{n,m}$, which is used to sum over, say, m. The remaining sum over n gives $\sum_n |S_F(E_n + \hbar\omega, E + \hbar\omega)|^2 = 1$. Therefore, what left is $\frac{e^2}{2h}\int_0^\infty dE R^2 f_1(E + \hbar\omega)$. Other terms are calculated by analogy.

The bilinear in Fermi functions f_1 and f_2 part reads,

$$\mathcal{P}_{33}^b(\omega) = -\frac{e^2}{h}\int dE \sum_{n,m,q=-\infty}^{\infty} \Big\{ RTf_2(E_q + \hbar\omega)f_1(E)S_F^*(E_n, E)S_F(E_m, E)\delta_{nq}\delta_{mq} +$$
$$R^2 f_1(E_q + \hbar\omega)f_1(E)S_F^*(E_n, E)S_F(E_m, E)S_F^*(E_m + \hbar\omega, E_q + \hbar\omega)S_F(E_n + \hbar\omega, E_q + \hbar\omega)$$
$$+TRf_1(E_q + \hbar\omega)f_2(E)\delta_{n0}\delta_{m0}S_F^*(E_m + \hbar\omega, E_q + \hbar\omega)S_F(E_n + \hbar\omega, E_q + \hbar\omega)$$
$$+T^2 f_2(E_q + \hbar\omega)f_2(E)\delta_{n0}\delta_{m0}\delta_{nq}\delta_{mq}\Big\}. \quad \text{(A9)}$$

Let us represent $\mathcal{P}_{33}^b(\omega) = \sum_{j=1}^4 B_j$ and calculate various terms separately. The first term is

$$B_1 = -\frac{e^2}{h}\int dE \sum_{n,m,q=-\infty}^{\infty} R^2 f_1(E_q + \hbar\omega)f_1(E)S_F^*(E_n, E)S_F^*(E_m + \hbar\omega, E_q + \hbar\omega)$$
$$\times S_F(E_m, E)S_F(E_n + \hbar\omega, E_q + \hbar\omega) = -R^2 v_\mu^2 e^2 \int_{-\mathcal{T}_0/2}^{\mathcal{T}_0/2} \frac{dt}{\mathcal{T}_0}\int_{-\infty}^{\infty} d\tau e^{i\omega\tau}\left|\mathcal{G}_1^{(1)}(t + \tau; t)\right|^2, \quad \text{(A10)}$$

where $\mathcal{G}_1^{(1)}$ is the first-order correlation function of the Fermi sea incoming from the first channel and modified by the source, see Equation (19). To prove the last line, I compute the time integral explicitly:

$$\int_0^{\mathcal{T}_0}\frac{dt}{\mathcal{T}_0}\int_{-\infty}^{\infty} d\tau e^{i\omega\tau}\left|\mathcal{G}_1^{(1)}(t + \tau; t)\right|^2 = \int_0^{\mathcal{T}_0}\frac{dt}{\mathcal{T}_0}\int_{-\infty}^{\infty} d\tau e^{i\omega\tau}\int\frac{dE}{h}f_1(E)e^{-\frac{i}{\hbar}E\tau}\sum_{n,m=-\infty}^{\infty} e^{-i\Omega n\tau}$$
$$\times e^{-i\Omega(n-m)t}S_F(E_n, E)S_F^*(E_m, E)\int\frac{dE'}{h}f_1(E')e^{\frac{i}{\hbar}E'\tau}$$
$$\sum_{q,\ell=-\infty}^{\infty} e^{i\Omega q\tau}e^{i\Omega(q-\ell)t}S_F^*\left(E_q', E'\right)S_F\left(E_\ell', E'\right) =$$

(the integration over t gives $q - \ell = n - m$, which I use to sum up over $\ell = q - n + m$)

$$= \int_{-\infty}^{\infty} d\tau e^{i\omega\tau}\int\frac{dE}{h}f_1(E)e^{-\frac{i}{\hbar}E\tau}\sum_{n,m,q=-\infty}^{\infty} e^{-i\Omega n\tau}$$
$$S_F(E_n, E)S_F^*(E_m, E)\int\frac{dE'}{h}f_1(E')e^{\frac{i}{\hbar}E'\tau}e^{i\Omega q\tau}S_F^*\left(E_q', E'\right)S_F\left(E_{q-n+m}', E'\right).$$

The integration over τ gives $h\delta\left(\hbar\omega - E_n + E_q'\right)$, which I use to integrate out $E_n = E_q' + \hbar\omega$,

$$\sim f_1\left(E_{q-n}' + \hbar\omega\right)f_1(E')S_F^*\left(E_q', E'\right)S_F\left(E_{q-n+m}', E'\right)$$
$$\times S_F^*\left(E_{q-n+m}' + \hbar\omega, E_{q-n}' + \hbar\omega\right)S_F\left(E_q' + \hbar\omega, E_{q-n}' + \hbar\omega\right).$$

Additionally I shift $q - n \to q$,

$$\sim f_1\left(E_q' + \hbar\omega\right)f_1(E')S_F^*\left(E_{q+n}', E'\right)S_F\left(E_{q+m}', E'\right)$$
$$\times S_F^*\left(E_{q+m}' + \hbar\omega, E_q' + \hbar\omega\right)S_F\left(E_{q+n}' + \hbar\omega, E_q' + \hbar\omega\right),$$

and finally, I shift $q+n \to n$ and $q+m \to m$ and get the same integrand as in Equation (A10) (up to $E' \to E$),

$$\begin{aligned} &\sim f_1\Big(E'_q+\hbar\omega\Big) f_1\big(E'\big) S_F^*\big(E'_n, E'\big) S_F\big(E'_m, E'\big) \\ &\times S_F^*\Big(E'_m+\hbar\omega, E'_q+\hbar\omega\Big) S_F\Big(E'_n+\hbar\omega, E'_q+\hbar\omega\Big). \end{aligned}$$

Other terms are calculated in the same way,

$$\begin{aligned} B_2 &= -\frac{e^2}{h}\int dE \sum_{q=-\infty}^{\infty} RTf_2(E_q+\hbar\omega) f_1(E) \big|S_F(E_q, E)\big|^2 \\ &= -RTv_\mu^2 e^2 \int_{-\mathcal{T}_0/2}^{\mathcal{T}_0/2} \frac{dt}{\mathcal{T}_0} \int_{-\infty}^{\infty} d\tau e^{i\omega\tau} \mathcal{G}_1^{(1)}(t+\tau; t) \mathcal{G}_{0,2}^{(1)*}(\tau), \end{aligned} \tag{A11}$$

$$\begin{aligned} B_3 &= -\frac{e^2}{h}\int dE \sum_{q=-\infty}^{\infty} TRf_1(E_q+\hbar\omega) f_2(E) \big|S_F(E+\hbar\omega, E_q+\hbar\omega)\big|^2 \\ &= -TRv_\mu^2 e^2 \int_{-\mathcal{T}_0/2}^{\mathcal{T}_0/2} \frac{dt}{\mathcal{T}_0} \int_{-\infty}^{\infty} d\tau e^{i\omega\tau} \mathcal{G}_{0,2}^{(1)}(\tau) \mathcal{G}_1^{(1)*}(t+\tau; t), \end{aligned} \tag{A12}$$

$$B_4 = -\frac{e^2}{h}\int dE T^2 f_2(E+\hbar\omega) f_2(E) = -T^2 v_\mu^2 e^2 \int_{-\mathcal{T}_0/2}^{\mathcal{T}_0/2} \frac{dt}{\mathcal{T}_0} \int_{-\infty}^{\infty} d\tau e^{i\omega\tau} \Big|\mathcal{G}_{0,2}^{(1)}(\tau)\Big|^2 .1 \tag{A13}$$

Putting all the terms together I get

$$\mathcal{P}_{33}^b(\omega) = -v_\mu^2 e^2 \int_0^{\mathcal{T}_0} \frac{dt}{\mathcal{T}_0} \int_{-\infty}^{\infty} d\tau e^{i\omega\tau} \Big|R\mathcal{G}_1^{(1)}(t+\tau; t) + T\mathcal{G}_{0,2}^{(1)}(\tau)\Big|^2. \tag{A14}$$

Note that when the second channel is also fed by a source, we need to replace the correlation function of the Fermi sea in equilibrium, $\mathcal{G}_{0,2}^{(1)}$, by the one modified by the source, $\mathcal{G}_2^{(1)}$.

Strictly speaking, both $\mathcal{P}_{33}^l(\omega)$, Equation (A7), and $\mathcal{P}_{33}^b(\omega)$, Equation (A14) diverge due to the infinite number of electrons that make up the Fermi sea, which contribute to them. However, their sum is finite. This sum is not zero even if the source is switched off. Therefore, to see the effect of injected electrons, we need to look at the excess noise. For this, I first calculate the noise when the source is off, $\mathcal{P}_{33}^{off}$, and then calculate the excess noise as the difference, $\mathcal{P}_{33}^{ex} = \mathcal{P}_{33} - \mathcal{P}_{33}^{off}$.

Appendix B.1.1. Equilibrium Noise, $\mathcal{P}_{33}^{off}$

For the sake of simplicity, I assume all the reservoirs have the same Fermi energy, $\mu_\alpha = \mu, \forall\alpha$ but possibly different temperatures. If necessary, the constant bias V_α at lead α, that is, $\mu_\alpha = \mu + eV_\alpha$, can be accounted for via an energy-independent scattering amplitude $S_\alpha = e^{i\frac{eV_\alpha}{\hbar}t}$.

To demonstrate that the equilibrium auto-correlation noise is not zero, I proceed as follows. I replace $\mathcal{G}_1$ by $\mathcal{G}_{0,1}$ in Equation (A14) for $\mathcal{P}^b_{33}$, use Equation (A7) for $\mathcal{P}^l_{33}$, which remains unchanged, use the following equation (see Equation (A13) and alike),

$$\frac{1}{h}\int dE\left\{F_{\alpha\beta}(E,E+\hbar\omega)-\frac{f_\alpha(E)+f_\beta(E+\hbar\omega)}{2}\right\}= \\ =-v_\mu^2\int\limits_{-\mathcal{T}_0/2}^{\mathcal{T}_0/2}\frac{dt}{\mathcal{T}_0}\int\limits_{-\infty}^{\infty}d\tau e^{i\omega\tau}\mathcal{G}^{(1)}_{0,\alpha}(\tau)\mathcal{G}^{(1)*}_{0,\beta}(\tau), \tag{A15}$$

and get the total equilibrium noise according to Equation (A5),

$$\begin{aligned}\mathcal{P}^{off}_{33}(\omega) &= \frac{e^2}{h}\int dE\Big\{F_{33}(E,E+\hbar\omega)+R^2F_{11}(E+\hbar\omega,E)+TRF_{21}(E+\hbar\omega,E)\\ &\quad +RTF_{12}(E+\hbar\omega,E)+T^2F_{22}(E+\hbar\omega,E)\Big\}.\end{aligned} \tag{A16}$$

Then, I transform

$$\begin{aligned}F_{\alpha\beta}(E,E+\hbar\omega)+F_{\beta\alpha}(E,E+\hbar\omega) &= F_{\alpha\alpha}(E,E+\hbar\omega)+F_{\beta\beta}(E,E+\hbar\omega)+\Phi_{\alpha\beta},\\ \Phi_{\alpha\beta} &= \big[f_\alpha(E)-f_\beta(E)\big]\big[f_\alpha(E+\hbar\omega)-f_\beta(E+\hbar\omega)\big],\end{aligned}$$

and integrate over energy using the following equations,

$$\int dEF_{\alpha\alpha}(E,E+\hbar\omega) = \frac{\hbar\omega}{2}\coth\frac{\hbar\omega}{2k_B\theta_\alpha}, \tag{A17}$$

$$\begin{aligned}\Xi\Big(\theta_\alpha,\theta_\beta,\omega\Big) &= \frac{1}{k_B\Big(\theta_\alpha+\theta_\beta\Big)}\int dE\Phi_{\alpha\beta}=\\ &= \frac{2\theta_\alpha}{\theta_\alpha+\theta_\beta}\int\limits_0^1 dx\frac{x\Big([x\Omega]^{\frac{\theta_\alpha}{\theta_\beta}-1}-1\Big)\Big(\big[\frac{x}{\Omega}\big]^{\frac{\theta_\alpha}{\theta_\beta}-1}-1\Big)}{(1+x\Omega)\Big(1+[x\Omega]^{\frac{\theta_\alpha}{\theta_\beta}}\Big)(1+\frac{x}{\Omega})\Big(1+\big[\frac{x}{\Omega}\big]^{\frac{\theta_\alpha}{\theta_\beta}}\Big)},\end{aligned}$$

where $\Omega=e^{-\frac{\hbar\omega}{2k_B\theta_\alpha}}$ and k_B is the Boltzmann constant. Finally, I represent $\mathcal{P}^{off}_{33}$ as follows,

$$\begin{aligned}\mathcal{P}^{off}_{33}(\omega) &= \frac{e^2}{h}k_B\Big\{\theta_3\xi\Big(\frac{\hbar\omega}{2k_B\theta_3}\Big)+R\theta_1\xi\Big(\frac{\hbar\omega}{2k_B\theta_1}\Big)\\ &\quad +T\theta_2\xi\Big(\frac{\hbar\omega}{2k_B\theta_2}\Big)+RT(\theta_1+\theta_2)\Xi(\theta_1,\theta_2,\omega)\Big\},\end{aligned} \tag{A18}$$

where $\xi(x)=x\coth x$.

The term with factor $\Xi(\theta_1,\theta_2,\omega)$ describes the auto-correlation thermal noise due to both terminals. It is shown in Figure A2.

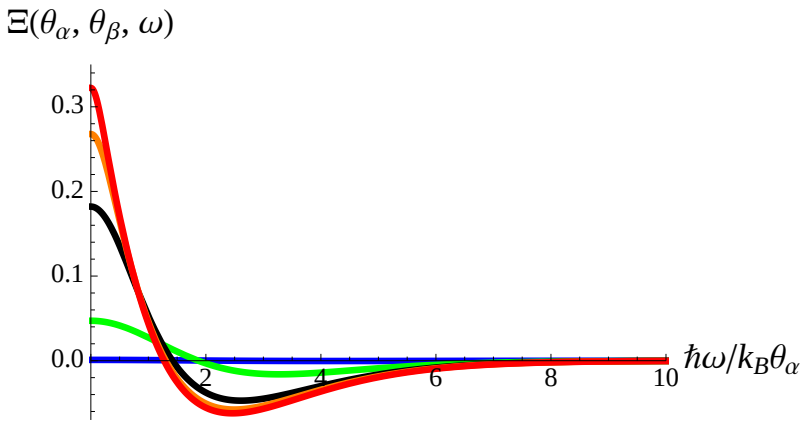

Figure A2. The joint two terminal contribution to the thermal noise $\Xi\left(\theta_\alpha, \theta_\beta, \omega\right)$, see Equations (A17) and (A18), is shown as a function of frequency at $\theta_\alpha/\theta_\beta = 1.1$ (blue), 2 (green), 5 (black), 10 (orange), and 20 (red).

Note that $\Xi\left(\theta_\alpha, \theta_\beta, \omega\right)$ is zero at $\theta_\alpha = \theta_\beta$, and as a function of ω it changes a sign from positive to negative with increasing ω. This sign change occurs around $\hbar\omega = k_B\left(\theta_\alpha + \theta_\beta\right)$. At this temperature/frequency, the joint two terminal contribution to thermal noise vanishes.

Appendix B.1.2. Excess Noise, $\mathcal{P}^{ex}_{33}$

I express the excess auto-correlation noise directly in terms of electron correlation functions $\mathcal{G}_\beta$ and $\mathcal{G}_{0,\beta}$. For this I note that the electronic source affects $\mathcal{P}^{b}_{33}$, Equation (A14), but leaves $\mathcal{P}^{l}_{33}$, Equation (A7), unchanged. Therefore, $\mathcal{P}^{ex}_{33} = \mathcal{P}^{b}_{33} - \mathcal{P}^{b,off}_{33}$,

$$\begin{aligned}\mathcal{P}^{ex}_{33}(\omega) &= e^2 v_\mu^2 \int_0^{\mathcal{T}_0} \frac{dt}{\mathcal{T}_0} \int_{-\infty}^{\infty} d\tau e^{i\omega\tau} \Big\{ \Big| R\mathcal{G}^{(1)}_{0,1}(t+\tau;t) + T\mathcal{G}^{(1)}_{0,2}(\tau) \Big|^2 \\ &\quad - \Big| R\mathcal{G}^{(1)}_{1}(t+\tau;t) + T\mathcal{G}^{(1)}_{0,2}(\tau) \Big|^2 \Big\}. \end{aligned} \tag{A19}$$

When both incoming channels are at the same temperature, $\theta_1 = \theta_2 \equiv \theta$, and have the same Fermi energies, $\mu_1 = \mu_2 \equiv \mu$, that is, their equilibrium correlation functions are the same, $\mathcal{G}_{0,1} = \mathcal{G}_{0,2} \equiv \mathcal{G}_0$, the above equation is simplified (see Equation (22a)).

$$\begin{aligned}\mathcal{P}^{ex}_{33}(\omega) &= e^2 v_\mu^2 \int_0^{\mathcal{T}_0} \frac{dt}{\mathcal{T}_0} \int_{-\infty}^{\infty} d\tau e^{i\omega\tau} \Big\{ -R^2 \Big| G^{(1)}_{1}(t+\tau;t) \Big|^2 \\ &\quad - 2R\,\mathrm{Re} G^{(1)}_{1}(t+\tau;t) \mathcal{G}^{(1)*}_{0}(\tau) \Big\}, \end{aligned} \tag{A20}$$

where

$$G^{(1)}_{1}(t+\tau;t) = \mathcal{G}^{(1)}_{1}(t+\tau;t) - \mathcal{G}^{(1)}_{0,1}(\tau). \tag{A21}$$

is the excess first-order correlation function injected by the source.

Appendix B.2. Cross-Correlation Nose

The cross-correlation noise in terms of $\mathcal{G}^{(1)}$ was given in [51],

$$\mathcal{P}_{34}(\omega) = -RTe^2v_\mu^2\int_0^{\mathcal{T}_0}\frac{dt}{\mathcal{T}_0}\int_{-\infty}^{\infty}d\tau e^{i\omega\tau}\left|\mathcal{G}_1^{(1)}(t+\tau;t)-\mathcal{G}_{0,2}^{(1)}(\tau)\right|^2. \tag{A22}$$

The excess cross-correlation noise, $\mathcal{P}_{34}^{ex}=\mathcal{P}_{34}-\mathcal{P}_{34}^{off}$, reads

$$\begin{aligned}\mathcal{P}_{34}^{ex}(\omega) = RTe^2v_\mu^2\int_0^{\mathcal{T}_0}\frac{dt}{\mathcal{T}_0}\int_{-\infty}^{\infty}d\tau e^{i\omega\tau}\Bigg\{&\left|\mathcal{G}_{0,1}^{(1)}(\tau)-\mathcal{G}_{0,2}^{(1)}(\tau)\right|^2\\ &-\left|\mathcal{G}_1^{(1)}(t+\tau;t)-\mathcal{G}_{0,2}^{(1)}(\tau)\right|^2\Bigg\}.\end{aligned} \tag{A23}$$

If both incoming channels are under the same conditions, $\mathcal{G}_{0,1}=\mathcal{G}_{0,2}\equiv\mathcal{G}_0$, then, unlike the auto-correlation noise, the cross-correlation noise has no equilibrium contribution and it is expressed solely in terms of the excess correlation function $G^{(1)}$ (see Equation (22b)):

$$\mathcal{P}_{34}(\omega) = \mathcal{P}_{34}^{ex}(\omega) = -RTe^2v_\mu^2\int_0^{\mathcal{T}_0}\frac{dt}{\mathcal{T}_0}\int_{-\infty}^{\infty}d\tau e^{i\omega\tau}\left|G_1^{(1)}(t+\tau;t)\right|^2. \tag{A24}$$

Appendix B.3. The Excess Noise Conservation at Zero Frequency

Conservation of charge imposes strong restrictions on zero frequency noise [14]. Namely, in the case under consideration, $\mathcal{P}_{33}^{ex}(0)$ and $\mathcal{P}_{34}^{ex}(0)$ are perfectly anti-correlated, such that

$$\mathcal{P}_{33}^{ex}(0)+\mathcal{P}_{34}^{ex}(0)=0. \tag{A25}$$

To show this, let us use Equations (A19) and (A23) in the above equation and obtain

$$\int_{-\mathcal{T}_0/2}^{\mathcal{T}_0/2}\frac{dt}{\mathcal{T}_0}\int_{-\infty}^{\infty}d\tau\left|\mathcal{G}_1^{(1)}(t+\tau;t)\right|^2=\int_0^{\mathcal{T}_0}\frac{dt}{\mathcal{T}_0}\int_{-\infty}^{\infty}d\tau\left|\mathcal{G}_{0,1}^{(1)}(\tau)\right|^2. \tag{A26}$$

Then, I use Equations (19) and (20) and calculate the right hand side in the above equation,

$$r.h.s.=\frac{1}{hv_\mu^2}\int dEf_1^2(E), \tag{A27}$$

and the left hand side,

$$l.h.s.=\frac{1}{hv_\mu^2}\int dE\sum_{n,m,q}f_1\Big(E_q\Big)f_1(E)S_F^*(E_n,E)S_F(E_m,E)S_F^*\Big(E_m,E_q\Big)S_F\Big(E_n,E_q\Big). \tag{A28}$$

Using the unitarity of the Floquet scattering amplitude of the source in the above equation, see Equations (13) and (A8), I sum over n and m and get the following:

$$l.h.s.=\frac{1}{hv_\mu^2}\int dEf_1^2(E)=r.h.s., \tag{A29}$$

that is, Equation (A26) is proven.

Appendix B.4. Noise and the Outgoing Correlation Matrix of a Linear Electronic Circuit

To generalize equations that relate electrical noise to electron correlation functions to the case with several sources and/or with several outgoing channels, it is instructive to combine correlation functions of all incoming channels into a square matrix $\hat{\mathcal{G}}^{(1)}_{in}$, and of all outgoing channels into a square matrix $\hat{\mathcal{G}}^{(1)}_{out}$, see in [44] for details. Their dimensions are equal to the number of incoming and outgoing channels, respectively. Let us denote by $\hat{S}$ the scattering matrix of a stationary electronic circuit connecting incoming and outgoing channels. If $\hat{S}$ is independent of energy, the incoming and outgoing correlation matrix are related as follows, $\hat{\mathcal{G}}^{(1)}_{out}(t_1;t_2) = \hat{S}^{*}\hat{\mathcal{G}}^{(1)}_{in}(t_1;t_2)\hat{S}^{T}$, where the upper index $*$ means complex conjugation, and T means transposition. As the incoming channels are not correlated, $\hat{\mathcal{G}}^{(1)}_{in}$ is diagonal.

In the case of a single QPC considered in this work, $\mathcal{G}^{(1)}_{in,11} = \mathcal{G}^{(1)}_{1}$, $\mathcal{G}^{(1)}_{in,22} = \mathcal{G}^{(1)}_{2}$, and two other elements are zero. The circuit's scattering matrix is given in Equation (17), $\hat{S} = \hat{S}^{QPC}$. Then, the outgoing correlation matrix reads

$$\hat{\mathcal{G}}^{(1)}_{out} = \begin{pmatrix} R\mathcal{G}^{(1)}_{1} + T\mathcal{G}^{(1)}_{2} & i\sqrt{RT}\left(\mathcal{G}^{(1)}_{1} - \mathcal{G}^{(1)}_{2}\right) \\ i\sqrt{RT}\left(\mathcal{G}^{(1)}_{2} - \mathcal{G}^{(1)}_{1}\right) & T\mathcal{G}^{(1)}_{1} + R\mathcal{G}^{(1)}_{2} \end{pmatrix}. \tag{A30}$$

Comparing the elements of $\hat{\mathcal{G}}^{(1)}_{out}$ to Equations (A19) and (A23), we can relate the excess noise and the elements of the outgoing correlation matrix as follows:

$$\mathcal{P}^{ex}_{\alpha\alpha'}(\omega) = e^2 \int_0^{\mathcal{T}_0} \frac{dt}{\mathcal{T}_0} \int_{-\infty}^{\infty} d\tau e^{i\omega\tau} \left\{ \left| v_\mu \mathcal{G}^{(1),off}_{out,\alpha\alpha'}(t+\tau;t) \right|^2 - \left| v_\mu \mathcal{G}^{(1)}_{out,\alpha\alpha'}(t+\tau;t) \right|^2 \right\}, \tag{A31}$$

where the upper index off indicates that electronic sources are switched off.

Notice that in the above equation, the indices α and α' number outgoing channels only; therefore, $\alpha, \alpha' = 1, 2$. While in Equations (A19) and (A23), the outgoing channels were numbered together with incoming channels, thus the outgoing channels were 3 and 4, respectively. Equation (A31) is applicable for any number of electronic sources and any number of outgoing channels.

Equations (A30) and (A31) illustrate why the auto- and cross-correlation noise are generally different. In particular, there is no cross-correlation noise in equilibrium (the off-diagonal terms in Equation (A30) vanish), but autocorrelation noise is present (the diagonal terms in Equation (A30) are not zero). Ultimately, this difference is due to the fact that fermionic operators in different leads anti-commute, but do not anti-commute in one lead.

Appendix C. Noise Caused by an Electron Injected from a Quantum Level Raising at a Constant Rapidity at Zero Temperature

In this appendix, I derive Equation (28) starting from Equations (22a) and (22b).

First, I use the wave function $\psi^{(c)}$ from Equation (6) and calculate the excess correlation function:

$$G^{(1)}(t+\tau;t) = \frac{e^{i\frac{\mu}{\hbar}\tau}}{\pi\Gamma_\tau v_\mu} \int_0^{\infty} dx e^{-x} e^{ix\frac{t+\tau}{\Gamma_\tau}} e^{-ix^2\zeta} \int_0^{\infty} dy e^{-y} e^{-iy\frac{t}{\Gamma_\tau}} e^{iy^2\zeta}. \tag{A32}$$

Here, I introduced the parameter of non-adiabaticity $\zeta = \tau_D/\Gamma_\tau$. This parameter controls the symmetry of the density profile of the injected wave packet [43]. With a symmetric density profile, injection is classified as adiabatic, with an asymmetric density profile, injection is non-adiabatic [46]. At $\zeta = 0$, this source is identical to the source of levitons, that is, $\psi^c = \psi^L$, see Equation (4) for ψ^L.

At the next step, let us calculate separately two terms entering Equations (22a) and (22b). I assume $\Gamma_\tau \ll \mathcal{T}_0$ and, therefore, extend the limits of integration over t to infinity.

Appendix C.1. The Term with $-v_\mu^2 G_1^{(1)} \mathcal{G}_0^{(1)*}$

I denote this term as Π_1. Using Equation (20) for $\mathcal{G}_0^{(1)}$ at zero temperature, I have

$$\begin{aligned} \Pi_1(\omega) &= -\int_{-\infty}^{\infty} d\tau e^{i\omega\tau} 2\mathrm{Re}\frac{\mathcal{C}(\tau)}{-2\pi i\tau}, \\ \mathcal{C}(\tau) &= \frac{1}{\pi\Gamma_\tau}\int_{-\infty}^{\infty} dt \int_0^{\infty} dx e^{-x} e^{ix\frac{t+\tau}{\Gamma_\tau}} e^{-ix^2\zeta} \int_0^{\infty} dy e^{-y} e^{-iy\frac{t}{\Gamma_\tau}} e^{iy^2\zeta}, \end{aligned} \tag{A33}$$

First, I evaluate coherence $\mathcal{C}(\tau)$. For this, I integrate over t,

$$\int_{-\infty}^{\infty} dt e^{ix\frac{t}{\Gamma_\tau}} e^{-iy\frac{t}{\Gamma_\tau}} = 2\pi\Gamma_\tau\delta(x-y).$$

This allows us to integrate, say, over y (the result is independent of the parameter of non-adiabaticity ζ),

$$\mathcal{C}(\tau) = 2\int_0^{\infty} dx e^{-2x} e^{i\frac{x}{\Gamma_\tau}\tau} = \frac{1}{1-i\tau/(2\Gamma_\tau)}. \tag{A34}$$

Substituting the above equation into Equation (A33), I calculate

$$\Pi_1(\omega) = e^{-|\omega|2\Gamma_\tau}. \tag{A35}$$

Note that namely this term determines the auto-correlation noise at $R \ll 1$: $\mathcal{P}_{33}^{ex}(\omega) \approx R\left(e^2/\mathcal{T}_0\right)\Pi_1(\omega)$, see Equation (7).

Appendix C.2. The Term with $v_\mu^2\left|G^{(1)}\right|^2$

I denote this term as Π_2,

$$\Pi_2(\omega) = \int_{-\infty}^{\infty} dt \int_{-\infty}^{\infty} d\tau e^{i\omega\tau}\left|\psi^{(c)}(t+\tau)\right|^2\left|\psi^{(c)}(t)\right|^2. \tag{A36}$$

First, I shift $\tau + t \to \tau$ and represent the above equation as the square of the Fourier transform of the wave packet density, $\Pi_2(\omega) = |\mathcal{N}(\omega)|^2$, where

$$\begin{aligned} \mathcal{N}(\omega) &= \Gamma_\tau \int_{-\infty}^{\infty} dz e^{i\omega\Gamma_\tau z}\left|\psi^{(c)}(\Gamma_\tau z)\right|^2 \\ &= \frac{1}{\pi}\int_{-\infty}^{\infty} dz e^{i\omega\Gamma_\tau z} \int_0^{\infty} dx e^{-x} e^{ixz} e^{-ix^2\zeta} \int_0^{\infty} dy e^{-y} e^{-iyz} e^{iy^2\zeta}, \end{aligned} \tag{A37}$$

where $z = \tau/\Gamma_\tau$. The integration over z gives,

$$\int_{-\infty}^{\infty} dz e^{i\omega\Gamma_\tau z} e^{ixz} e^{-iyz} = 2\pi\delta(\omega\Gamma_\tau + x - y).$$

Then, I integrate over $y = x + \omega\Gamma_\tau$ (for positive ω),

$$\mathcal{N}(\omega) = 2e^{i(\omega\Gamma_\tau)^2\zeta} e^{-\omega\Gamma_\tau} \int_0^{\infty} dx e^{-2x} e^{i2x\omega\Gamma_\tau\zeta} = e^{i(\omega\Gamma_\tau)^2\zeta} \frac{e^{-\omega\Gamma_\tau}}{1 - i\omega\Gamma_\tau\zeta},$$

and obtain (for arbitrary ω),

$$\Pi_2(\omega) = \frac{e^{-|\omega|2\Gamma_\tau}}{1 + (\omega\tau_D)^2}, \tag{A38}$$

where $\tau_D = \Gamma_\tau\zeta$. This term fully defines cross-correlation noise and partially auto-correlation noise.

Appendix C.3. Excess Noise Power

By combining both terms together, I get

$$\begin{aligned} \mathcal{P}_{33}^{ex}(\omega) &= R\frac{e^2}{\mathcal{T}_0}\Pi_1(\omega) - R^2\frac{e^2}{\mathcal{T}_0}\Pi_2(\omega) \\ \mathcal{P}_{34}(\omega) &= -RT\frac{e^2}{\mathcal{T}_0}\Pi_2(\omega). \end{aligned} \tag{A39}$$

Using Equations (A35) and (A38) we arrive at Equation (28).

Note that at $\omega = 0$, $\Pi_1(0) = \Pi_2(0)$ and $\mathcal{P}_{33}^{ex}(0) + \mathcal{P}_{34}(0) = 0$, in agreement with Equation (A25).

Appendix D. Noise Caused by an Electron Injected from a Quantum Level Raising at a Constant Rapidity at Non-Zero Temperature

In this appendix, I repeat the calculations presented in the previous Appendix, but at non-zero temperatures, and compute the temperature-dependent factor $\eta(\omega, \theta)$ from Equation (29).

For this model, the correlation function of electrons injected at a nonzero temperature, $\theta > 0$, was expressed in terms of the correlation function at zero temperature in [60].

$$G_{1,\theta}^{(1)}(t+\tau;t) = \int d\epsilon \left(-\frac{\partial f_1}{\partial\epsilon}\right) e^{i\frac{\epsilon}{\hbar}\tau} G_{1,0}^{(1)}\left(t+\tau-\frac{\epsilon}{c};t-\frac{\epsilon}{c}\right). \tag{A40}$$

Here, the indices θ and 0 refer to non-zero and zero temperatures, respectively, f_1 is the Fermi distribution function for electrons with temperature θ in lead 1, which the additional electron is injected into, $G_{1,0}^{(1)}$ is given in Equation (A32), and the rapidity $c = \hbar/(2\tau_D\Gamma_\tau)$, see $\psi^{(c)}$, Equation (6).

The above equation can be interpreted as the correlation function for a single-particle mixed quantum state. Each component of this mixed state is characterized by the correlation functions $e^{i\frac{\epsilon}{\hbar}\tau} G_{1,0}^{(1)}\left(t+\tau-\frac{\epsilon}{c};t-\frac{\epsilon}{c}\right)$. The components of this mixed state are distributed according to the thermal probability density $p(\epsilon) = -\partial f_1(\epsilon)/\partial\epsilon$.

Appendix D.1. The Term with $-v_\mu^2 G_1^{(1)} \mathcal{G}_0^{(1)*}$

Using Equations (20) and (A40), I calculate

$$\begin{aligned}\Pi_1(\omega) &= \frac{1}{\pi}\int\limits_{-\infty}^{\infty} d\tau e^{i\omega\tau}\frac{1/\tau_\theta}{\sinh(\tau/\tau_\theta)}\mathrm{Im}\int d\epsilon e^{i\frac{\epsilon}{\hbar}}\left(-\frac{\partial f_1}{\partial\epsilon}\right)\mathcal{C}(\tau),\\ \mathcal{C}(\tau) &= \int\limits_{-\infty}^{\infty} dt e^{-i\frac{\mu}{\hbar}\tau} v_\mu G_{1,0}^{(1)}\left(t-\frac{\epsilon}{c}+\tau; t-\frac{\epsilon}{c}\right).\end{aligned} \tag{A41}$$

As energy ϵ and time t enter $G_{1,0}^{(1)}$ as a difference, $t-\epsilon/c$, the correlation function calculated at zero temperature and integrated over time, $\mathcal{C}(\tau)$, becomes independent of ϵ. This property allows us to integrate out ϵ,

$$\Pi_1(\omega) = \int\limits_{-\infty}^{\infty} d\tau e^{i\omega\tau}\left(\frac{\tau/\tau_\theta}{\sinh(\tau/\tau_\theta)}\right)^2\frac{\mathrm{Im}[\mathcal{C}(\tau)]}{\pi\tau}. \tag{A42}$$

With $G_{1,0}^{(1)}$ from Equation (A32), I calculate $\mathcal{C}(\tau)$ as described above in Appendix C.1 and find

$$\Pi_1(\omega) = \frac{1}{2\pi\Gamma_\tau}\int\limits_{-\infty}^{\infty} d\tau e^{i\omega\tau}\left(\frac{\tau/\tau_\theta}{\sinh(\tau/\tau_\theta)}\right)^2\frac{1}{1+\tau^2/(2\Gamma_\tau)^2}. \tag{A43}$$

Remind that the thermal coherence time $\tau_\theta = \hbar/(\pi k_B\theta_1)$. At $\theta_1 = 0$, we recover Equation (A35). Note that $\Pi_1(\omega)$ obeys Equation (27).

Appendix D.2. The Term with $v_\mu^2\left|G^{(1)}\right|^2$

At non-zero temperature the corresponding term reads

$$\Pi_2(\omega) = \iint d\epsilon d\epsilon' p(\epsilon)p(\epsilon')|\mathcal{N}_{\epsilon-\epsilon'}(\omega)|^2. \tag{A44}$$

Here, the thermal probability density $p(\epsilon) = -\partial f_1(\epsilon)/\partial\epsilon$, and

$$\mathcal{N}_{\epsilon-\epsilon'}(\omega) = \int\limits_{-\infty}^{\infty}\frac{dz}{\pi}e^{i\left(\omega+\frac{\epsilon-\epsilon'}{\hbar}\right)\Gamma_\tau z}\int\limits_0^\infty dx e^{-x}e^{ix\left(z-\frac{\epsilon}{c\Gamma_\tau}\right)}e^{-ix^2\zeta}\int\limits_0^\infty dy e^{-y}e^{-iy\left(z-\frac{\epsilon'}{c\Gamma_\tau}\right)}e^{iy^2\zeta}, \tag{A45}$$

where $z = \tau/\Gamma_\tau$. Up to an irrelevant phase factor, $\mathcal{N}_{\epsilon-\epsilon'}(\omega)$ is the same as $\mathcal{N}\left(\omega+\frac{\epsilon-\epsilon'}{\hbar}\right)$ from Equation (A37). Therefore, we can write

$$\Pi_2(\omega) = \frac{1}{1+(\omega\tau_D)^2}\iint d\epsilon d\epsilon' p(\epsilon)p(\epsilon')e^{-\left|\omega+\frac{\epsilon-\epsilon'}{\hbar}\right|2\Gamma_\tau}. \tag{A46}$$

To bring the above equation into the form close to Π_1, Equation (A43), let us represent the exponential factor as follows,

$$e^{-\left|\omega+\frac{\epsilon-\epsilon'}{\hbar}\right|2\Gamma_\tau} = \frac{1}{2\pi\Gamma_\tau}\int\limits_{-\infty}^{\infty} d\tau\frac{e^{i\left(\omega+\frac{\epsilon-\epsilon'}{\hbar}\right)\tau}}{1+\tau^2/(2\Gamma_\tau)^2}.$$

Then, we can integrate over ϵ and ϵ' in Equation (A46) as follows,

$$\int d\epsilon p(\epsilon) e^{i\frac{\epsilon}{\hbar}\tau} = \frac{\tau/\tau_\theta}{\sinh(\tau/\tau_\theta)},$$

and find that

$$\Pi_2(\omega) = \frac{1}{1+(\omega\tau_D)^2} \int_{-\infty}^{\infty} \frac{d\tau e^{i\omega\tau}}{2\pi\Gamma_\tau} \frac{\left(\frac{\tau/\tau_\theta}{\sinh(\tau/\tau_\theta)}\right)^2}{1+\tau^2/(2\Gamma_\tau)^2} = \frac{\Pi_1(\omega)}{1+(\omega\tau_D)^2}, \tag{A47}$$

where Π_1 is given in Equation (A43).

Notice that we cannot use the inverse Fourier transformation with respect to ω in order to express $\Pi_2(\omega)$ at temperature θ in terms of $\Pi_2(\omega)$ at zero temperature. As a result, the excess noise, Equation (A39), does not obey Equation (27).

Appendix D.3. Excess Noise Power

The relation between $\Pi_2(\omega)$ and $\Pi_1(\omega)$, Equation (A47), is independent on temperature. Therefore, the effect of temperature on $\Pi_2(\omega)$ is the same as on $\Pi_1(\omega)$, see Equation (A43). Then, we use Equations (A43) and (A47) in Equation (A39) and generalize Equation (28) to the case of non-zero temperatures,

$$\begin{aligned} \mathcal{P}^{ex}_{33}(\omega) &= R\frac{e^2}{\mathcal{T}_0}\frac{T+(\omega\tau_D)^2}{1+(\omega\tau_D)^2} e^{-|\omega|2\Gamma_\tau}\eta(\omega,\theta), \\ \mathcal{P}_{34}(\omega) &= -R\frac{e^2}{\mathcal{T}_0}\frac{T}{1+(\omega\tau_D)^2} e^{-|\omega|2\Gamma_\tau}\eta(\omega,\theta), \end{aligned} \tag{A48}$$

where

$$\eta(\omega,\theta) = e^{|\omega|2\Gamma_\tau} \int_{-\infty}^{\infty} \frac{d\tau e^{i\omega\tau}}{2\pi\Gamma_\tau} \frac{\left(\frac{\tau/\tau_\theta}{\sinh(\tau/\tau_\theta)}\right)^2}{1+\tau^2/(2\Gamma_\tau)^2}. \tag{A49}$$

This factor is shown in Equation (29), where I introduced $x = \tau/(2\Gamma_\tau)$.

References

1. Jullien, T.; Roulleau, P.; Roche, B.; Cavanna, A.; Jin, Y.; Glattli, D.C. Quantum tomography of an electron. *Nature* **2014**, *514*, 603–607. [CrossRef] [PubMed]
2. Bisognin, R.; Marguerite, A.; Roussel, B.; Kumar, M.; Cabart, C.; Chapdelaine, C.; Mohammad-Djafari, A.; Berroir, J.M.; Bocquillon, E.; Plaçais, B.; et al. Quantum tomography of electrical currents. *Nat. Commun.* **2019**, *10*, 3379. [CrossRef] [PubMed]
3. Bocquillon, E.; Parmentier, F.D.; Grenier, C.; Berroir, J.M.; Degiovanni, P.; Glattli, D.C.; Plaçais, B.; Cavanna, A.; Jin, Y.; Fève, G. Electron Quantum Optics: Partitioning Electrons One by One. *Phys. Rev. Lett.* **2012**, *108*, 196803. [CrossRef]
4. Dubois, J.; Jullien, T.; Portier, F.; Roche, P.; Cavanna, A.; Jin, Y.; Wegscheider, W.; Roulleau, P.; Glattli, D.C. Minimal-excitation states for electron quantum optics using levitons. *Nature* **2013**, *502*, 659–663. [CrossRef] [PubMed]
5. Bocquillon, E.; Freulon, V.; Berroir, J.M.; Degiovanni, P.; Plaçais, B.; Cavanna, A.; Jin, Y.; Fève, G. Coherence and Indistinguishability of Single Electrons Emitted by Independent Sources. *Science* **2013**, *339*, 1054–1057. [CrossRef]
6. Marguerite, A.; Bocquillon, E.; Berroir, J.M.; Plaçais, B.; Cavanna, A.; Jin, Y.; Degiovanni, P.; Fève, G. Two-particle interferometry in quantum Hall edge channels. *Phys. Status Solidi* **2016**, *254*, 1600618. [CrossRef]
7. Glattli, D.C.; Roulleau, P.S. Levitons for electron quantum optics. *Phys. Status Solidi* **2016**, *254*, 1600650. [CrossRef]
8. Mahé, A.; Parmentier, F.D.; Bocquillon, E.; Berroir, J.M.; Glattli, D.C.; Kontos, T.; Plaçais, B.; Fève, G.; Cavanna, A.; Jin, Y. Current correlations of an on-demand single-electron emitter. *Phys. Rev. B* **2010**, *82*, 201309. [CrossRef]
9. Parmentier, F.D.; Bocquillon, E.; Berroir, J.M.; Glattli, D.C.; Plaçais, B.; Fève, G.; Albert, M.; Flindt, C.; Büttiker, M. Current noise spectrum of a single-particle emitter: Theory and experiment. *Phys. Rev. B* **2012**, *85*, 165438. [CrossRef]
10. Maire, N.; Hohls, F.; Kaestner, B.; Pierz, K.; Schumacher, H.W.; Haug, R.J. Noise measurement of a quantized charge pump. *Appl. Phys. Lett.* **2008**, *92*, 082112. [CrossRef]

11. Gabelli, J.; Thibault, K.; Gasse, G.; Lupien, C.; Reulet, B. Characterization and control of charge transfer in a tunnel junction. *Phys. Status Solidi* **2017**, *254*, 1600619. [CrossRef]
12. Landauer, R. The noise is the signal. *Nature* **1998**, *392*, 658–659. [CrossRef]
13. Reznikov, M.; de Picciotto, R.; Heiblum, M.; Glattli, D.C.; Kumar, A.; Saminadayar, L. Quantum shot noise. *Superlattices Microstruct.* **1998**, *23*, 901–915. [CrossRef]
14. Blanter, Y.; Büttiker, M. Shot noise in mesoscopic conductors. *Phys. Rep.* **2000**, *336*, 1–166. [CrossRef]
15. Fletcher, J.D.; Johnson, N.; Locane, E.; See, P.; Griffiths, J.P.; Farrer, I.; Ritchie, D.A.; Brouwer, P.W.; Kashcheyevs, V.; Kataoka, M. Continuous-variable tomography of solitary electrons. *Nat. Commun.* **2019**, *10*, 1355. [CrossRef] [PubMed]
16. Albert, M.; Flindt, C.; Büttiker, M. Accuracy of the quantum capacitor as a single-electron source. *Phys. Rev. B* **2010**, *82*, 041407. [CrossRef]
17. Grenier, C.; Hervé, R.; Fève, G.; Degiovanni, P. Electron quantum optics in quantum hall edge channels. *Mod. Phys. Lett. B* **2011**, *25*, 1053–1073. [CrossRef]
18. Grenier, C.; Hervé, R.; Bocquillon, E.; Parmentier, F.D.; Plaçais, B.; Berroir, J.M.; Fève, G.; Degiovanni, P. Single-electron quantum tomography in quantum Hall edge channels. *New J. Phys.* **2011**, *13*, 093007. [CrossRef]
19. Dubois, J.; Jullien, T.; Grenier, C.; Degiovanni, P.; Roulleau, P.; Glattli, D.C. Integer and fractional charge Lorentzian voltage pulses analyzed in the framework of photon-assisted shot noise. *Phys. Rev. B* **2013**, *88*, 085301. [CrossRef]
20. Grenier, C.; Dubois, J.; Jullien, T.; Roulleau, P.; Glattli, D.C.; Degiovanni, P. Fractionalization of minimal excitations in integer quantum Hall edge channels. *Phys. Rev. B* **2013**, *88*, 085302. [CrossRef]
21. Ferraro, D.; Feller, A.; Ghibaudo, A.; Thibierge, E.; Bocquillon, E.; Fève, G.; Grenier, C.; Degiovanni, P. Wigner function approach to single electron coherence in quantum Hall edge channels. *Phys. Rev. B* **2013**, *88*, 205303. [CrossRef]
22. Thibierge, E.; Ferraro, D.; Roussel, B.; Cabart, C.; Marguerite, A.; Fève, G.; Degiovanni, P. Two-electron coherence and its measurement in electron quantum optics. *Phys. Rev. B* **2016**, *93*, 081302. [CrossRef]
23. Gaury, B.; Waintal, X. A computational approach to quantum noise in time-dependent nanoelectronic devices. *Phys. E Low-Dimens. Syst. Nanostructures* **2016**, *75*, 72–76. [CrossRef]
24. Rech, J.; Ferraro, D.; Jonckheere, T.; Vannucci, L.; Sassetti, M.; Martin, T. Minimal Excitations in the Fractional Quantum Hall Regime. *Phys. Rev. Lett.* **2017**, *118*, 076801. [CrossRef] [PubMed]
25. Roussel, B.; Cabart, C.; Fève, G.; Thibierge, E.; Degiovanni, P. Electron quantum optics as quantum signal processing. *Phys. Status Solidi* **2017**, *254*, 1600621. [CrossRef]
26. Ferraro, D.; Ronetti, F.; Vannucci, L.; Acciai, M.; Rech, J.; Jockheere, T.; Martin, T.; Sassetti, M. Hong-Ou-Mandel characterization of multiply charged Levitons. *Eur. Phys. J. Spec. Top.* **2018**, *227*, 1345–1359. [CrossRef]
27. Misiorny, M.; Fève, G.; Splettstoesser, J. Shaping charge excitations in chiral edge states with a time-dependent gate voltage. *Phys. Rev. B* **2018**, *97*, 075426. [CrossRef]
28. Glattli, D.C.; Roulleau, P. Pseudorandom binary injection of levitons for electron quantum optics. *Phys. Rev. B* **2018**, *97*, 125407. [CrossRef]
29. Dittmann, N.; Splettstoesser, J. Finite-frequency noise of interacting single-electron emitters: Spectroscopy with higher noise harmonics. *Phys. Rev. B* **2018**, *98*, 115414. [CrossRef]
30. Rebora, G.; Acciai, M.; Ferraro, D.; Sassetti, M. Collisional interferometry of levitons in quantum Hall edge channels at ν=2. *Phys. Rev. B* **2020**, *101*, 245310. [CrossRef]
31. Yue, X.K.; Yin, Y. Quasiparticles states for integer- and fractional-charged electron wave packets. *arXiv* **2020**, arXiv:2004.00743 .
32. Roussel, B.; Cabart, C.; Fève, G.; Degiovanni, P. Processing quantum signals carried by electrical currents. *arXiv* **2020**, arXiv:2008.01580v1 .
33. Bäuerle, C.; Glattli, D.C.; Meunier, T.; Portier, F.; Roche, P.; Roulleau, P.; Takada, S.; Waintal, X. Coherent control of single electrons: A review of current progress. *Rep. Prog. Phys.* **2018**, *81*, 056503. [CrossRef] [PubMed]
34. Haack, G.; Moskalets, M.; Splettstoesser, J.; Büttiker, M. Coherence of single-electron sources from Mach-Zehnder interferometry. *Phys. Rev. B* **2011**, *84*, 081303. [CrossRef]
35. Haack, G.; Moskalets, M.; Büttiker, M. Glauber coherence of single-electron sources. *Phys. Rev. B* **2013**, *87*, 201302. [CrossRef]
36. Levitov, L.S.; Lee, H.; Lesovik, G.B. Electron counting statistics and coherent states of electric current. *J. Math. Phys.* **1996**, *37*, 4845–4866. [CrossRef]
37. Ivanov, D.A.; Lee, H.W.; Levitov, L.S. Coherent states of alternating current. *Phys. Rev. B* **1997**, *56*, 6839–6850. [CrossRef]
38. Flindt, C. Quantum physics: Single electrons pop out of the Fermi sea. *Nature* **2013**, *502*, 630–632. [CrossRef] [PubMed]
39. Keeling, J.; Klich, I.; Levitov, L.S. Minimal Excitation States of Electrons in One-Dimensional Wires. *Phys. Rev. Lett.* **2006**, *97*, 116403. [CrossRef] [PubMed]
40. Büttiker, M.; Thomas, H.; Prêtre, A. Mesoscopic capacitors. *Phys. Lett. A* **1993**, *180*, 364–369. [CrossRef]
41. Gabelli, J.; Fève, G.; Berroir, J.M.; Plaçais, B.; Cavanna, A.; Etienne, B.; Jin, Y.; Glattli, D.C. Violation of Kirchhoff's laws for a coherent RC circuit. *Science* **2006**, *313*, 499–502. [CrossRef] [PubMed]
42. Fève, G.; Mahé, A.; Berroir, J.M.; Kontos, T.; Plaçais, B.; Glattli, D.C.; Cavanna, A.; Etienne, B.; Jin, Y. An on-demand coherent single-electron source. *Science* **2007**, *316*, 1169–1172. [CrossRef] [PubMed]
43. Keeling, J.; Shytov, A.V.; Levitov, L.S. Coherent Particle Transfer in an On-Demand Single-Electron Source. *Phys. Rev. Lett.* **2008**, *101*, 196404. [CrossRef] [PubMed]

44. Moskalets, M.; Haack, G. Heat and charge transport measurements to access single-electron quantum characteristics. *Phys. Status Solidi* **2016**, *254*, 1600616–15. [CrossRef]
45. Filippone, M.; Marguerite, A.; Le Hur, K.; Fève, G.; Mora, C. Phase-Coherent Dynamics of Quantum Devices with Local Interactions. *Entropy* **2020**, *22*, 847. [CrossRef]
46. Moskalets, M.; Haack, G.; Büttiker, M. Single-electron source: Adiabatic versus nonadiabatic emission. *Phys. Rev. B* **2013**, *87*, 125429. [CrossRef]
47. Beenakker, C.W.J. Search for Majorana Fermions in Superconductors. *Annu. Rev. Condens. Matter Phys.* **2013**, *4*, 113–136. [CrossRef]
48. Aguado, R. Majorana quasiparticles in condensed matter. *La Rivista del Nuovo Cimento* **2017**, *40*, 523–593. [CrossRef]
49. Hassler, F.; Grabsch, A.; Pacholski, M.J.; Oriekhov, D.O.; Ovdat, O.; Adagideli, I.; Beenakker, C.W.J. Half-integer charge injection by a Josephson junction without excess noise. *Phys. Rev. B* **2020**, *102*, 045431. [CrossRef]
50. Moskalets, M. Fractionally Charged Zero-Energy Single-Particle Excitations in a Driven Fermi Sea. *Phys. Rev. Lett.* **2016**, *117*, 046801. [CrossRef] [PubMed]
51. Moskalets, M.; Haack, G. Single-electron coherence: Finite temperature versus pure dephasing. *Phys. E Low-Dimens. Syst. Nanostructures* **2016**, *75*, 358–369. [CrossRef]
52. Moskalets, M.; Kotilahti, J.; Burset, P.; Flindt, C. Composite two-particle sources. *Eur. Phys. J. Spec. Top.* **2020**, *229*, 647–662. [CrossRef]
53. Büttiker, M. Edge-State Physics Without Magnetic Fields. *Science* **2009**, *325*, 278–279. [CrossRef]
54. Büttiker, M. Scattering theory of thermal and excess noise in open conductors. *Phys. Rev. Lett.* **1990**, *65*, 2901–2904. [CrossRef] [PubMed]
55. Büttiker, M. Scattering theory of current and intensity noise correlations in conductors and wave guides. *Phys. Rev. B* **1992**, *46*, 12485–12507. [CrossRef] [PubMed]
56. Moskalets, M.; Büttiker, M. Floquet scattering theory of quantum pumps. *Phys. Rev. B* **2002**, *66*, 205320, [CrossRef]
57. Moskalets, M.; Büttiker, M. Time-resolved noise of adiabatic quantum pumps. *Phys. Rev. B* **2007**, *75*, 035315. [CrossRef]
58. Moskalets, M.; Büttiker, M. Spectroscopy of electron flows with single- and two-particle emitters. *Phys. Rev. B* **2011**, *83*, 035316. [CrossRef]
59. Burset, P.; Kotilahti, J.; Moskalets, M.; Flindt, C. Time-Domain Spectroscopy of Mesoscopic Conductors Using Voltage Pulses (Adv. Quantum Technol. 3-4/2019). *Adv. Quantum Technol.* **2019**, *2*, 1970023. [CrossRef]
60. Moskalets, M. Single-particle emission at finite temperatures. *Low Temp. Phys.* **2017**, *43*, 865–876. [CrossRef]
61. Moskalets, M. Single-particle shot noise at nonzero temperature. *Phys. Rev. B* **2017**, *96*, 165423. [CrossRef]
62. Bocquillon, E.; Freulon, V.; Parmentier, F.D.; Berroir, J.M.; Plaçais, B.; Wahl, C.; Rech, J.; Jonckheere, T.; Martin, T.; Grenier, C.; et al. Electron quantum optics in ballistic chiral conductors. *Ann. Der Phys.* **2014**, *526*, 1–30. [CrossRef]
63. Glattli, D.C.; Roulleau, P. Hanbury-Brown Twiss noise correlation with time controlled quasi-particles in ballistic quantum conductors. *Phys. E Low-Dimens. Syst. Nanostructures* **2016**, *76*, 216–222. [CrossRef]
64. Moskalets, M. Noise of a single-electron emitter. *Phys. Rev. B* **2013**, *88*, 035433. [CrossRef]